A pathological *RNASEH1* mutant causes R-loop depletion and aberrant DNA segregation in mitochondria

Gokhan Akman,[1Ψ] Radha Desai,[1Ψ] Laura Bailey,[2] Takehiro Yasukawa,[2#] Ilaria Dalla Rosa,[1] Romina Durigon,[1] John Bradley Holmes,[2,3] Chloe Moss,[1] Mara Mennuni,[1] Henry Houlden,[4] Robert J. Crouch,[3] Michael G. Hanna,[4] Robert D.S. Pitceathly,[4,5] Antonella Spinazzola,[1*] Ian J. Holt.[1,*]

1. MRC Laboratory, Mill Hill, London NW71AA, UK
2. MRC Mitochondrial Biology Unit, Cambridge, CB1 9SY, UK
3. Division of Developmental Biology, Eunice Kennedy Shriver National Institute of Child Health and Human Development, National Institutes of Health, Bethesda, Maryland 20892, USA.
4. MRC Centre for Neuromuscular Diseases, UCL Institute of Neurology and National Hospital for Neurology and Neurosurgery, Queen Square, London, WC1N 3BG, UK.
5. Department of Basic and Clinical Neuroscience, Institute of Psychiatry, Psychology and Neuroscience, King's College London, London, SE5 8AF, UK.

Ψ These two authors made an equal contribution to the study.

Present address: Department of Clinical Chemistry and Laboratory Medicine, Graduate School of Medical Sciences, Kyushu University, 3-1-1 Maidashi, Higashi-ku, Fukuoka 812-8582, Japan

*correspondence:
ian.holt@headoffice.mrc.ac.uk; antonella.spinazzola@crick.ac.uk

Abstract

The genetic information in mammalian mitochondrial DNA is densely packed; there are no introns and only one sizeable non-coding, or control, region containing key *cis*-elements for its replication and expression. Many molecules of mitochondrial DNA bear a third strand of DNA, known as 7S DNA, which forms a displacement (D-) loop in the control region. Here we show that many other molecules contain RNA as a third strand. The RNA of these R-loops maps to the control region of the mitochondrial DNA and is complementary to 7S DNA. Ribonuclease H1 is essential for mitochondrial DNA replication, it degrades RNA hybridized to DNA and so the R-loop is a potential substrate. In cells with a pathological variant of Ribonuclease H1 associated with mitochondrial disease, R-loops are of low abundance and there is mitochondrial DNA aggregation. These findings implicate Ribonuclease H1 and RNA in the physical segregation of mitochondrial DNA, perturbation of which represents a new disease mechanism.

Significance Statement

The DNA in mitochondria is essential for efficient energy production. Critical for mitochondrial DNA replication and expression are sequences concentrated in the so-called control region. We report that many mitochondrial DNAs contain a triple stranded region whose third strand is RNA and maps to the control region. These R-loops contribute to DNA architecture and replication in the mitochondria; and aberrant R-loop processing causes disease.

Introduction

Mammalian mitochondrial DNA (mtDNA) contributes thirteen critical proteins of the oxidative phosphorylation system that produces much of the cell's energy. Consequently, aberrant or insufficient mtDNA causes cell and tissue dysfunction that manifests in a range of human diseases (1). In most cells and tissues mtDNA is formed of circles of double-stranded DNA. The two strands are denoted heavy (H) and light (L) owing to their different base compositions. Important *cis*-elements that function as origins of replication, the replication terminus and transcriptional promoters, are concentrated in the control region (CR) (2-5). Many molecules of mtDNA bear a third strand of DNA, known as 7S DNA, which forms a displacement (D-) loop covering much of the CR. The D-loop spans approximately half a kilobase (kb) of the 16.5 kb of mammalian mtDNA (6-8) and is present on between 1% and 65% of mtDNA molecules (9). The frequent synthesis of 7S DNA across such a pivotal region of the mitochondrial genome implies an important role for the D-loop in mtDNA metabolism, and it has been implicated in protein recruitment and mtDNA organization (10, 11).

Ribonuclease H1 (RNase H1) degrades RNA hybridized to DNA (12) and is essential for mtDNA maintenance in mice (13). Recently, pathological mutations in RNASEH1, including *RNASEH1*, c.424G>A; p.Val142Ile (V142I), have been reported to cause adult onset neuromuscular disease (14). We have studied fibroblasts with V142I RNase H1 and find no evidence of the primer retention associated with loss of the gene in murine cells (15). However the human cells carrying mutant RNase H1 have markedly reduced levels of a newly identified RNA that forms an R-loop on the mtDNA. The RNA is similar in length and location to the D-loop, but complementary to 7S DNA. The low level of the mitochondrial R-loop is associated with aggregation of mtDNA, suggesting a role for it in mtDNA organization and segregation.

Results

Analysis of RNA hybridized to mtDNA has to contend with the ready degradation of the RNA during extraction (16). Previous analysis of fragments of mtDNA encompassing the control region (CR) demonstrated that they included molecules with 7S DNA as expected for triple stranded D-loops (10), but no RNA (*SI Appendix*, Fig. S1A). However, more recently, inter-strand cross-linking was found to preserve RNA/DNA hybrids of mtDNA and to enhance markedly the signal associated with D-loop-like structures ((17) and *SI Appendix*, Fig. S1B). Therefore we sought to determine whether the increased signal reflected RNA preservation or solely increased D-loop stability. As intact RNA/DNA hybrids are easier to isolate from solid tissues than from aneuploid cultured cells (17), we refined our isolation procedure for mouse liver mtDNA. The new protocol employs a protease treatment on ice (see Materials and Methods), which improves the quality of the mtDNA, as evidenced by the replication intermediates resolved by two-dimensional agarose gel-electrophoresis (2D-AGE) (*SI Appendix*, Fig. S2). The revised procedure was used for all subsequent analysis of murine mtDNA. To enrich D-loops and small bubble structures and to determine their nucleic acid composition, we gel-extracted material from the base of an initiation arc, treated it with RNase HI, DNase or no enzyme, prior to denaturation and 1D-AGE. Blot hybridization to strand-specific probes revealed L-strand RNA complementary to 7S DNA and of similar mobility and abundance (Fig. 1A). Analysis of smaller fragments containing the CR resolved the small bubble structures into two discrete species, **D** and **R,** of similar abundance (Fig. 1B). Ban2 (which cuts 7S DNA bound to mtDNA (i.e. the D-loop) (*SI Appendix*, Fig. S3A)) cleaved **D**, but not **R** (*SI Appendix*, Fig. S3B), indicating the latter was refractive to digestion at nucleotide position (np) 15,749 (in the control region), possibly owing to an RNA component, as restriction enzymes are unable to cleave RNA/DNA hybrids (e.g. (18)). Species **R** proved sensitive to *in vitro* RNase H treatment, but was largely insensitive to single-stranded RNase (RNase T_1) (Fig. 1C), indicating it contains an RNA hybridized to DNA for much of its length. Therefore, we conclude that species **D** contains the well-recognized D-loop, whereas **R** is a previously unknown form of mtDNA containing an R-loop, whose RNA is approximately the complement of the D-loop.

Further mtDNA preparations and gel extractions were performed to generate material for conversion of the R-loop RNA to DNA via reverse transcription (see Materials and Methods), and sequencing analysis confirmed that the R-loop maps to the CR (Fig. 2). Seven of 41 RNAs sequenced were oligo-adenylated (Table S1, Fig. 2), all at the terminus mapping closest to the light-strand promoter (LSP). Oligo or polyadenylation occurs at the 3′ end of mitochondrial and other messenger RNAs and so indicates that these RNAs are L-strand, concordant with the results of the strand-specific probes (Fig. 1A). The most frequent 3′ ends mapped precisely to LSP (20 of 41 sequences) and none extended beyond this point (Fig. 2, Table S1), suggesting LSP is the ultimate terminus for R-loop synthesis. Of the 41 R-loops sequenced, the eight longest (with respect to the inferred 5′ end) began at np 15476 ± 2 nt, within a region (np 15423-15483 (19)) predicted to form secondary structure (20), known as the Termination Associated Sequence (TAS) due to its proximity to the 3′ end of many 7S DNAs (8). Seventeen of the other 5′ ends were clustered around np 15,600, within 25 nucleotides of the second origin of replication in the CR, Ori-b (15). We propose to name the RNA component of the abundant mitochondrial R-loop LC-RNA (**L**ight- (or lagging-) strand, **C**ontrol region **RNA**), as the term 7S RNA has been applied to the transient primer sequence spanning LSP to Ori-H on the H-strand (15, 21).

Although the preservation of RNA/DNA hybrids in aneuploid cells is more difficult than in solid tissues in our experience (17), a similar pair of small bubble-like structures was evident in human mtDNA of 143B osteosarcoma cells subjected to inter-strand cross-linking (Fig. 3A); and species refractive to Ban2 digestion at np 15,749 of murine mtDNA (i.e. equivalent to species R of *SI Appendix*, Fig. S3B) were detected in heart, brain and kidney (*SI Appendix*, Fig. S4A). Hence, R-loops, as well as D-loops, appear to be a ubiquitous feature of mammalian mtDNA. Because the gel-extracted mouse mtDNA material contained both LC-RNA and 7S DNA (Fig. 1A), it was not clear whether the two species resided on different molecules; however, the greater resolution achieved with the smaller 1.35 kb restriction fragment indicated that the two small bubble-like structures (D and R) had similar mobility in the first-dimension electrophoresis step (Fig. 1B), suggesting their masses were substantially the same, as expected for species containing *either* 7S DNA *or* LC-RNA, but not both. This inference was

corroborated by the analysis of human mtDNA, as a specific replication (Y) fork structure marks the position where a species of ~2.1 kb of duplex DNA resolves, which is similar to that predicted for molecules containing both LC-RNA and 7S DNA, whereas species D and R ran considerably closer to the linear duplex fragments of 1.45 kb (see overlay in Fig. 3A). Moreover, the single-stranded DNA content of D and R is approximately the same, evidenced by the similar mobility shift when pre-incubated with single-stranded DNA binding protein, prior to gel fractionation (Fig. 3B, 3C). Nevertheless, a short initiation type arc of a length appropriate to a combined D/R loop was detectable in cross-linked rat liver mtDNA samples (*SI Appendix*, Fig. S4B), suggesting some molecules contain both LC-RNA and 7S DNA.

The existence of the mitochondrial R-loop raises questions about its formation and processing, and its roles in mtDNA metabolism. Concerning the enzyme involved in its processing, RNase H1 represents a strong candidate, as it is known to target RNA/DNA hybrids in the control region (15). The identification of a homozygous missense mutation in *RNASEH1*, (c.424G>A; p.Val142Ile (V142I)) in the affected members of two unrelated families with neuromuscular disease (*SI Appendix*, Fig. S5A and Table S2), offered an opportunity to explore the enzyme's impact on mtDNA and the mitochondrial R-loop, using patient-derived fibroblasts and muscle of affected individuals.

Recently we showed that murine cells lacking the enzyme are unable to maintain mtDNA (15). In contrast, fibroblasts carrying V142I RNase H1 had 92% of the average mtDNA copy number of three controls and normal levels of the mtDNA packaging protein TFAM (Fig. 4A). Concordant with the mtDNA copy number data, the RNase H1 variant, V142I, produces milder pathologies in humans than gene ablation in the mouse: adult-onset neuromuscular disease (encephalomyopathy) (this report and (14)), as oppose to embryonic lethality (13). However, analysis of the steady-state level of the protein using detergent-solubilized cell lysates, stored frozen, implied the V142I substitution resulted in almost complete loss of RNase H1, as the protein was barely detectable (Fig. 4B). This could indicate either a much greater redundancy for RNase H1 in humans than mice, or that the immunoblotting results were misleading. In favor of the latter

possibility, electrophoresis of freshly prepared samples, immediately after cell lysis, yielded a markedly higher signal for V142I RNase H1 than those stored frozen (Fig. 4C). Hence, we infer that the mutant protein is less stable than wild-type RNase H1, and the presence of an appreciable amount of RNase H1 protein in the patient-derived fibroblasts correlates with the less severe phenotype of the human disease compared to *Rnaseh1* excision in the mouse.

A prominent feature of the loss of RNase H1 in murine cells is the retention of primers on the mtDNA in the CR (15). It has long been proposed that 7S DNA arises from a primer initiating at the LSP and that the 5´ ends of the 7S DNAs mark the RNA-DNA transition point (22). Fractionation of 7S DNA from mouse embryonic fibroblasts (MEF) without *Rnaseh1* indicates it is contiguous with a segment of RNA, detected by a probe spanning LSP to Ori-H, whereas in cells retaining *Rnaseh1* the RNA extension is not detectable (Fig. 5A). Therefore, *Rnaseh1* ablation leads to (LSP-Ori-H) primer retention on 7S DNA molecules, as well as on productive nascent strands (15). Because 7S DNA is highly abundant it was chosen to determine whether the human mutant RNase H1 compromises primer processing in the CR of human mtDNA.

Before assessing 7S DNA primer retention in V142I RNase H1 fibroblasts, we first analyzed mitochondrial D-loop length and properties in human embryonic kidney (HEK) cells. Fractionation by sodium-borate gel-electrophoresis resolved four 7S DNA species of ~560-650 nucleotides, which are concordant with those defined previously (8) with free 5´ ends mapping to np 111, 150, 168 and 191 (23). Treatment with RNase HI did not alter their lengths (Fig. 5B) suggesting that none of the 7S DNAs had a retained primer (of 10 or more ribonucleotides). The lengths of the 7S DNAs of human fibroblasts with wild-type or mutant (V142I) RNase H1 were similar to those of HEK cells, irrespective of an in vitro RNase HI treatment (Fig. 5C). Therefore, in the human mutant fibroblasts, there was no evidence of retention of a primer from LSP to Ori-H, which would have extended the 7S DNAs by 200 nucleotides, one third of their usual length.

Because RNA/DNA hybrids of mtDNA can be lost readily during isolation (16, 24), we additionally carried out a ‘blocked site’ assay to screen for retained primers. In

MEF lacking *Rnaseh1*, the failure to remove the LSP-Ori-H primer creates a stretch of RNA/DNA hybrid in the mtDNA that is refractive to restriction digestion at a site (np 16,179), immediately downstream of LSP (np 16,190) (*SI Appendix*, Fig. S6A and (15)). Msc1 was selected for the equivalent analysis of human mtDNA, as its cleavage site, at np 323, lies between LSP (np 407) and Ori-H (multiple proposed sites at or downstream of np 300) (*SI Appendix*, Fig. S6B). First we applied the procedure to mtDNA of human 143B osteosarcoma cells, after silencing RNase H1 for 144 hours (as previously (25)). The experiment potentially served two purposes, providing a test for the hypothesis that RNase H1 performs the same role in human and murine cells, and if true, a positive control for RNA retention in human mtDNA. *RNASEH1* gene silencing in 143B cells markedly increased the amount of Msc1-digested mtDNA that was uncut at np 323 (but not at np 8939), particularly in cells subjected to psoralen/UV cross-linking that improves the recovery of RNA/DNA hybrids (17). Moreover, site blockage was largely relieved when the samples were co-incubated with Eco-RNase HI for the final hour of the restriction digestion (Fig. 5D). These findings suggest that an acute shortage of RNase H1 in human (143B) cells leads to the retention of the primer from LSP to the DNA transition site, as per murine fibroblasts (15). In contrast, the V142I RNase H1 was not associated with any detectable site blockage at np 323 of human mtDNA (Fig. 5E), again indicating there is no persistent primer from LSP to Ori-H in the patient-derived fibroblasts. Thus, human mitochondria containing the V142I RNase H1 are able to remove the primers associated with 7S DNA. Either the residual activity of the mutant enzyme (14) is sufficient for this task, or there is redundancy for primer processing in some human cell types but not in others.

The V142I mutation was associated with an approximately 8 fold increase in the abundance of 7S DNAs relative to control fibroblasts (Fig. 6A), as reported previously (14). The earlier report also measured a 2-4 fold increase in mitochondrial replication intermediates in the mutant fibroblasts detected by 2D gel-electrophoresis. However, very few products of strand-asynchronous/bootlace replication were detected (14), while they form the majority of mitochondrial replication intermediates in other cell types and in solid tissues (3, 18), and so their disintegration during extraction might have confounded the analysis. In a

different approach, we intentionally separated the strands of mtDNA after cleaving at np 14,955 (Xho1) or 14,445 (Bsu361), sites 1.7 and 2.2 kb downstream of the origin of replication, Ori-H, respectively. Fragments of these lengths, i.e. nascent strands of DNA with a 5´ end mapping to Ori-H, were approximately three times more abundant in RNase H1 mutant cells than control fibroblasts (Fig. 6A). Thus, the new finding establishes that mitochondrial replication intermediates are present at higher steady-state level in cells with V142I RNase H1, and the increase in nascent strands suggests this is attributable to slow mtDNA replication rather than slow turnover of the mtDNA. As with the 7S DNAs (Fig. 5C), there was no evidence of a retained primer associated with the nascent strands of mtDNA in V142I RNase H1 fibroblasts (Fig. 6B, S6C), in contrast to murine cells lacking RNase H1 (15).

In terms of our prior knowledge of mtDNA replication and maintenance, it was difficult to explain the marked increase in 7S DNA caused by mutant RNase H1 (Fig. 6A), as the only candidate substrate, the so-called 7S RNA (primer), appears to be processed normally in cells with V142I RNase H1 (Figs. 5, 6B and S6C). Assuming RNase H1 acts exclusively on RNA/DNA hybrids and doesn't have an unrecognized function, 7S DNA levels must be influenced by RNA other than 7S RNA (the primer spanning LSP to Ori-H). The mitochondrial R-loop is a clear alternative candidate. As a test of the potential impact of V142I RNase H1 on the mitochondrial R-loop, we again employed a blocked site assay, by digesting human fibroblast DNA with Acc1 and Ban2 (Fig. 6C). Human mtDNA has an Acc1 site at np 15,255, approximately 850 nt downstream of the 3´ end of the D-loop. Ban2 has two sites in the D-loop region of human mtDNA (and extrapolating from the mouse data (Fig. 2) also in the R-loop) at np 16459 and 40, and a third outside the CR at np 629. Hence, the R-loop should prevent cleavage by Ban2 at np 16,459 and 40, generating a fragment of 1.95 kb. (D-loops, on the other hand, are susceptible to Ban2 digestion (*SI Appendix*, Fig. S3). A species commensurate with a fragment containing blocked sites at np 16459 and 40 was readily detectable in HEK cells and in control fibroblasts, whereas this species was of markedly lower abundance in the V142I RNase H1 fibroblasts (and in cells expressing high levels of recombinant Twinkle DNA helicase) (Fig. 6C). The mitochondrial R-loop, resolved by 2D-AGE analysis of mtDNA after inter-strand

cross-linking, was also of lower abundance in V142I RNase H1 containing fibroblasts than controls (*SI Appendix*, Fig. S7). Hence, the fibroblasts of the patient with mutant RNase H1 had fewer R-loops than control fibroblasts.

The high abundance of mitochondrial R-loops in normal cells and tissues and the maintenance of near normal mtDNA copy number when it is scarce (see Figs. 1, 4A, 6C and S7) suggested that many R-loops are not directly involved in replication. The portion of the mtDNA including the control region is implicated in the association of the mtDNA to the inner mitochondrial membrane (26), and we have described multi-copy fragments of mtDNA encompassing the CR, held together by protein, that are putative intermediates of the segregation process. These findings led us to propose that the D-loop is involved in the organization and segregation of mtDNA (10, 11); the same inferences apply to the mitochondrial R-loop. Therefore, we determined the distribution and organization of mtDNA in fibroblasts with mutant and wild-type RNase H1. Immunocytochemistry showed that over one-third of the mutant primary fibroblasts have abnormally large mtDNA foci (nucleoids) (Fig. 7A and *SI Appendix*, Fig. S8), occupying as much as 200 times the volume of the typical (modal) mtDNA foci of control fibroblasts. Deconvolution analysis of the microscope images revealed closely packed smaller discrete foci of approximately 0.3 μm in diameter (Fig. 7B), similar to those of the control fibroblasts analyzed here and previously (27), leading us to infer that the enlarged mtDNA foci comprise clusters of single copies of mtDNA. The multipartite nature of the enlarged mitochondrial nucleoids suggests that RNase H1 V142I impedes the physical segregation of mtDNA molecules. Attribution of the enlarged nucleoid phenotype to the pathological variant of RNase H1 is supported by the observations that loss of RNase H1 in murine fibroblasts or its depletion in human 143B cells also result in the formation of abnormally large mtDNA foci (*SI Appendix*, Fig. S9). The inability to distribute mtDNA normally is associated with perturbation of the mitochondrial network, as the mitochondria themselves form dense bodies around the aggregates of mtDNA (Fig. 7C). Hence, the distribution of mtDNA and mitochondria might be coupled. Despite the aggregation of nucleoids and mitochondria the clusters of mtDNAs remained replication competent, as labeling of cellular DNA for a period of 10 hours with the nucleotide

analogue bromo-deoxyuridine (BrdU) and immunocytochemistry to the incorporated BrdU produced a similar staining profile as anti-DNA labeling (Fig. 7D). Mitochondrial disease manifests in non-dividing cells, and so quiescent cells potentially offered a context closer to that of the affected tissues (muscle and brain). After stopping cell growth via serum starvation, mtDNA foci were larger than in the corresponding proliferating cells; in the case of the patient-derived cells the clusters of mtDNA reached a size and DNA concentration that was visible with DAPI staining, in contrast to control cells (Fig. 8A). Next, we extended the analysis of mtDNA organization to muscle sections and found that clustering was also evident in an affected tissue, muscle, and the distribution of mtDNA foci was not as uniform as control fibers (Fig. 8B and *SI Appendix*, Fig. S10). Mitochondrial DNA clustering and disorganization were evident in a majority of the patient's muscle fibers, whereas only a small percentage displayed mitochondrial proliferation based on succinate dehydrogenase staining (*SI Appendix*, Fig. S5-Bii). Therefore, the enlarged mtDNA foci are attributable to impaired segregation and not a secondary consequence of mitochondrial biogenesis and proliferation.

In the cultured cells with V142I RNase H1 there is no evident perturbation of transcription based on the steady-state levels of four mature mitochondrial transcripts, nor was there an increase in precursor RNAs, suggesting that RNA processing is not compromised in the mutant fibroblasts (*SI Appendix*, Fig. S11). However, the mitochondria of V142I RNase H1 fibroblasts displayed rates of protein synthesis a third lower than controls (with the exception of ATP synthase subunit A6 that gave inconsistent results), as evidenced by ^{35}S-methionine labeling of mitochondrial translation products (Fig. 9A), and their respiratory capacity was compromised (Fig. 9B). These defects might relate to perturbation of the intimate connections between the translation machinery and the mtDNA (28), perhaps because the mitochondrial R-loop includes a putative ribosome-binding sequence (21).

Discussion

The discovery of pathological mutations in human RNase H1 advances our understanding of mitochondrial disorders and highlights the fundamental role of the enzyme and RNA in mtDNA metabolism. The pathology associated with the human mutation and the loss of RNase H1 activity in the mouse is strikingly different. *Rnaseh1* ablation is incompatible with development beyond early embryogenesis (13), whereas the missense mutation in *RNASEH1* results in an adult-onset neuromuscular disease. The molecular defects also differ: an absence of murine RNase H1 results in mtDNA depletion and primer retention (15), but neither is the case for the human mutant RNase H1 (Figs. 4A and 5). Two striking changes in the mtDNA of cells harboring V142I RNase H1 are the increase in D-loops and the decrease in the newly recognized R-loop.

The detection of the mitochondrial R-loop comes almost half a century after the first descriptions of the mitochondrial D-loop (6, 7). Both are triple stranded species with the third strand located in the major non-coding region, which is frequently described as the least conserved part of the mitochondrial genome; however, apart from three short hypervariable regions (29) most of the CR is well conserved, and the portion known as the conserved central domain (8, 20) defines much of the overlap between the D-loop and the R-loop (Fig. 2). The high abundance and location of the triple stranded species and the perturbations described in this report, combined with earlier studies of the D-loop, suggest they have important roles in mitochondrial DNA maintenance and expression.

The V142I substitution results in lower RNase H activity than the wild-type enzyme (14), yet is associated with a marked decrease in R-loops in the fibroblasts of the patient studied here (Fig. 6C, S7). Human cells might activate a back-up mechanism of processing RNA/DNA hybrids in response to RNase H1 deficiency, but with poorer powers of discrimination, causing the mitochondrial R-loop to be dislodged and degraded prematurely. However, the V142I RNase H1 protein appears to be unstable (Fig. 4B, 4C), potentially owing to its susceptibility to oxidation (30), raising the intriguing possibility that the mutant protein is modified *in vivo* to accelerate its turnover, or to render it inactive (30), in order to

prevent a dominant negative phenotype manifesting. This would be desirable if the V142I substitution disrupted RNase H1's interaction with a protein partner(s) that restricted its actions. Even at 40% of full activity (14), unregulated V142I RNase H1 would be expected to degrade RNA/DNA hybrids inappropriately, and could thereby increase the rate of turnover of mitochondrial R-loops. All that said, definitive demonstration that R-loop depletion is the result of V142I RNase H1 awaits the creation of a cellular or animal model with this mutation.

The increase in the abundance of D-loops in cells with mutant RNase H1 can be explained in one of two ways. The D-loop is the precursor of the mitochondrial R-loop. Thus, more D-loops are made to increase R-loop synthesis enabling some R-loops to survive long enough to perform its (critical) function(s); i.e. to compensate for unfettered RNase H1 (V142I) degrading the mitochondrial R-loop rapidly, or accelerated R-loop turnover due to an imperfect substitute for the mutant enzyme. Alternatively, the reciprocal relationship between the D-loop and the R-loop in the fibroblasts carrying mutant RNase H1 could be owing to overlapping functions. D-loops might not be optimal for mtDNA segregation but be serviceable when R-loops are scarce, although the increase in D-loops appears disproportionate. Further study of the D-loop could help to resolve its relationship to the R-loop; if D-loops beget R-loops then decreasing the level of D-loops in the fibroblasts with mutant RNase H1 would decrease R-loop levels still further, and situations that result in a decrease in D-loops would be accompanied by a decrease in R-loops, or increased R-loop stability.

The impact of RNase H1 on mtDNA segregation strongly implies RNA involvement. Such a role might have been anticipated earlier, as mitochondria retain features of their prokaryotic ancestors, and in bacteria RNA has long been proposed to play an important role in nucleoid organization (31). Furthermore, RNA polymerase has been linked to bacterial chromosomal segregation (32). Thus, the mtDNA aggregates of V142I RNase H1 cells, formed when the abundance of mitochondrial R-loops is low, potentially point to an analogous arrangement and process in the mitochondria, in which RNase H1 is required to process products of the mitochondrial RNA polymerase (POLRMT) to facilitate mtDNA segregation.

There are two ways in which POLRMT could generate the mitochondrial R-loop. To produce all the mature RNAs required for gene expression the polycistronic H-strand transcript must cover almost the entire mitochondrial genome (33); the furthest from the promoter, $tRNA^{Thr}$, is separated from the CR by the anti-sense sequence of $tRNA^{Pro}$. Thus, POLRMT needs to extend synthesis of the minimal H-strand polycistronic RNA only a short distance beyond $tRNA^{Thr}$ to enter the CR and create a RNA corresponding to the mitochondrial R-loop. The other means by which POLRMT could readily generate the mitochondrial R-loop is via promoter-independent synthesis on the single-stranded template formed by the D-loop. The site in the CR known as Ori-b is a good candidate, it functions as a start point for DNA synthesis on both strands (3, 15), presumably preceded by a short primer in the case of the L-strand, and over 40% of the sequenced R-loops have a 5´ end within 25 nucleotides of Ori-b (Fig. 2). Any triplex regions of DNA in the D-loop would be disrupted in the process of LC-RNA synthesis, reducing the stability of the 7S DNA, and so facilitating its removal, leaving the mitochondrial R-loop. This can readily be achieved given that RNA/DNA hybrids have higher melting temperatures than equivalent duplex DNAs, and a number of DNA helicases are poor at unwinding RNA/DNA duplexes (34). Both methods of generating R-loops might exist for different purposes. H-strand polycistronic transcripts offer the possibility of transcript-dependent (aka Bootlace) replication, or TDR (17), as, according to the model, RNA is hybridized to the lagging strand template from its inception. Hence, a prediction of TDR is that it requires an RNA covering much of the CR (i.e. LC-RNA). However, the D-loop dependent R-loops starting at TAS or Ori-b, would leave a small gap to any H-strand polycistronic transcripts that terminate outside the CR (HSP-transcript in Fig. 2), which might prevent their use in TDR. This hypothesis in turn suggests a possible tight coupling of transcription and replication, in which they are consecutive, not concurrent, events. Viz. H-strand transcription initiates at the heavy strand promoter and proceeds around the mtDNA terminating at LSP, with the final portion of the transcript serving as the (lagging-strand) initiator RNA for TDR. Some form of coupling between the D-loop and the longest polycistronic HSP transcripts was inferred in 1990, as 7S DNA levels correlate with those of the most HSP-distal (cytochrome *b*) mRNA (9).

In both the schemes for POLRMT-mediated synthesis of R-loops, the putative cloverleaf structure known as TAS could play a key regulatory role. Binding of a protein to TAS could arrest transcription (in the manner of mTERF at a another site in the mitochondrial genome (35)), and thereby prevent POLRMT progression into the CR, denying the mtDNA the first RNA needed for transcript-dependent replication. In the case of R-loop synthesis via the D-loop, TAS could facilitate recruitment of POLRMT or other accessory factors to the appropriate start site. POLG2 is an excellent candidate for binding to TAS, based on its D-loop binding properties (10) and homology to amino acyl-tRNA-synthetases (36). Furthermore the mitochondrial R-loops have a displaced DNA strand that binds single-stranded DNA binding protein (Fig. 3B), which suggests a new role for mtSSB in mtDNA maintenance.

The discovery of the mitochondrial R-loop may necessitate a reassessment of almost all aspects of mtDNA metabolism. As R-loops are low in the cells of a patient with mutant RNase H1 and mtDNA abnormalities, investigation of the abundance and behavior of the mitochondrial R-loop in the context of pathological mutants of Twinkle DNA helicase (37), MGME1 (38), FARS2 (39), FBXL4 (40) and POLG (41) could prove informative. Human cultured cells are an appropriate model system for the study of this and many other aspects of mtDNA replication and maintenance. For a protracted period it was thought that cultured cells did not recapitulate the prominent mtDNA abnormalities (depletion or multiple deletions) seen in the tissues of patients. However, although proliferating cultured cells of patients with defects in deoxynucleotide metabolism display normal mtDNA levels, in most cases mtDNA depletion occurs when they exit the cell cycle (e.g. (42, 43)), and a revaluation of the phenomenon of multiple deletions suggests they too are present in cultured cells. The existing data from muscle samples are consistent with the view that multiple deletions are broken replication intermediates. It is possible, even likely, that most of these are intact prior to extraction, as linear DNA molecules are unlikely to persist for long, given the dangers of strand invasion and the aberrant recombination products they could generate. Thus, the accumulated replication intermediates seen in the mutant RNase H1 fibroblasts (Fig. 6A) could be directly related to the multiple deletions

detected in the muscle of the patient; however, their contribution to the pathology in this and the allied disorders remains to be established.

Materials and Methods

Full methods are described in SI Appendix. MtDNA from tissue was prepared as described previously (17) but without a 50ºC incubation step. Digestion and fractionation of native or denatured mtDNA was as previously (15, 17). Mitochondrial translation was via ^{35}S-methionine labeling in the presence of emetine (44), and oxygen consumption was measured using a XF flux analyzer. Control region RNA was sequenced after reverse transcription and cloning. MEF mtDNAs were prepared as described previously (15). Cell culture, RNA interference, mitochondrial DNA isolation, nucleic acid digestion, modification, and analysis were as described previously (15, 17, 25, 45). This study was performed under the ethical guidelines issued by University College London for clinical studies. Written informed consent was obtained from all subjects before genetic testing.

FUNDING

J. Bradley Holmes was an NIH-CamGrad Scholar (2006-2010). Mara Mennuni is supported by the European Commission. The study was funded by the Medical Research Council (intramural award to IJH, and a senior non-clinical fellowship to AS); RDSP, HH and MGH are supported by an MRC Centre for Neuromuscular Diseases grant (G0601943), the UK NHS Specialised Service for Rare Mitochondrial Diseases of Adults and Children and the NIHR UCLH/UCL Biomedical Research Centre. RJC is supported by the National Institutes of Health (Intramural Research Program of the Eunice Kennedy Shriver National Institute of Child Health and Human Development).

References

1. Area-Gomez E & Schon EA (2014) Mitochondrial genetics and disease. *Journal of child neurology* 29(9):1208-1215.
2. Kasamatsu H & Vinograd J (1973) Unidirectionality of replication in mouse mitochondrial DNA. *Nat New Biol* 241(108):103-105.
3. Yasukawa T, Yang MY, Jacobs HT, & Holt IJ (2005) A bidirectional origin of replication maps to the major noncoding region of human mitochondrial DNA. *Mol Cell* 18(6):651-662.
4. Fish J, Raule N, & Attardi G (2004) Discovery of a major D-loop replication origin reveals two modes of human mtDNA synthesis. *Science* 306(5704):2098-2101.
5. Chang DD & Clayton DA (1986) Precise assignment of the light-strand promoter of mouse mitochondrial DNA: a functional promoter consists of multiple upstream domains. *Mol Cell Biol* 6(9):3253-3261.
6. Arnberg A, van Bruggen EF, & Borst P (1971) The presence of DNA molecules with a displacement loop in standard mitochondrial DNA preparations. *Biochim Biophys Acta* 246(2):353-357.
7. Kasamatsu H, Robberson DL, & Vinograd J (1971) A novel closed-circular mitochondrial DNA with properties of a replicating intermediate. *Proc Natl Acad Sci U S A* 68(9):2252-2257.
8. Walberg MW & Clayton DA (1981) Sequence and properties of the human KB cell and mouse L cell D-loop regions of mitochondrial DNA. *Nucleic Acids Res* 9(20):5411-5421.
9. Annex BH & Williams RS (1990) Mitochondrial DNA structure and expression in specialized subtypes of mammalian striated muscle. *Mol Cell Biol* 10(11):5671-5678.
10. Di Re M*, et al.* (2009) The accessory subunit of mitochondrial DNA polymerase gamma determines the DNA content of mitochondrial nucleoids in human cultured cells. *Nucleic Acids Res* 37(17):5701-5713.
11. He J*, et al.* (2007) The AAA+ protein ATAD3 has displacement loop binding properties and is involved in mitochondrial nucleoid organization. *J Cell Biol* 176(2):141-146.
12. Keller W & Crouch R (1972) Degradation of DNA RNA hybrids by ribonuclease H and DNA polymerases of cellular and viral origin. *Proc Natl Acad Sci U S A* 69(11):3360-3364.
13. Cerritelli SM*, et al.* (2003) Failure to produce mitochondrial DNA results in embryonic lethality in Rnaseh1 null mice. *Mol Cell* 11(3):807-815.
14. Reyes A*, et al.* (2015) RNASEH1 Mutations Impair mtDNA Replication and Cause Adult-Onset Mitochondrial Encephalomyopathy. *Am J Hum Genet* 97(1):186-193.
15. Holmes JB*, et al.* (2015) Primer retention owing to the absence of RNase H1 is catastrophic for mitochondrial DNA replication. *Proc Natl Acad Sci U S A* 112(30):9334-9339.
16. Pohjoismaki JL*, et al.* (2010) Mammalian mitochondrial DNA replication intermediates are essentially duplex but contain extensive tracts of RNA/DNA hybrid. *J Mol Biol* 397(5):1144-1155.
17. Reyes A*, et al.* (2013) Mitochondrial DNA replication proceeds via a 'bootlace' mechanism involving the incorporation of processed transcripts. *Nucleic Acids Res* 41(11):5837-5850.

18. Yasukawa T*, et al.* (2006) Replication of vertebrate mitochondrial DNA entails transient ribonucleotide incorporation throughout the lagging strand. *EMBO J* 25(22):5358-5371.
19. Bayona-Bafaluy MP*, et al.* (2003) Revisiting the mouse mitochondrial DNA sequence. *Nucleic Acids Res* 31(18):5349-5355.
20. Brown GG, Gadaleta G, Pepe G, Saccone C, & Sbisa E (1986) Structural conservation and variation in the D-loop-containing region of vertebrate mitochondrial DNA. *J Mol Biol* 192(3):503-511.
21. Ojala D, Crews S, Montoya J, Gelfand R, & Attardi G (1981) A small polyadenylated RNA (7 S RNA), containing a putative ribosome attachment site, maps near the origin of human mitochondrial DNA replication. *J Mol Biol* 150(2):303-314.
22. Clayton DA (1982) Replication of animal mitochondrial DNA. *Cell* 28(1):693-705.
23. Kang D, Miyako K, Kai Y, Irie T, & Takeshige K (1997) In vivo determination of replication origins of human mitochondrial DNA by ligation-mediated polymerase chain reaction. *J Biol Chem* 272:15275-15279.
24. Yang MY*, et al.* (2002) Biased incorporation of ribonucleotides on the mitochondrial L-strand accounts for apparent strand-asymmetric DNA replication. *Cell* 111(4):495-505.
25. Ruhanen H, Ushakov K, & Yasukawa T (2011) Involvement of DNA ligase III and ribonuclease H1 in mitochondrial DNA replication in cultured human cells. *Biochim Biophys Acta* 1813(12):2000-2007.
26. Albring M, Griffith J, & Attardi G (1977) Association of a protein structure of probable membrane derivation with HeLa cell mitochondrial DNA near its origin of replication. *Proc Natl Acad Sci U S A* 74(4):1348-1352.
27. Kukat C*, et al.* (2011) Super-resolution microscopy reveals that mammalian mitochondrial nucleoids have a uniform size and frequently contain a single copy of mtDNA. *Proc Natl Acad Sci U S A* 108(33):13534-13539.
28. He J*, et al.* (2012) Human C4orf14 interacts with the mitochondrial nucleoid and is involved in the biogenesis of the small mitochondrial ribosomal subunit. *Nucleic Acids Res* 40(13):6097-6108.
29. Lutz S, Weisser HJ, Heizmann J, & Pollak S (1997) A third hypervariable region in the human mitochondrial D-loop. *Human Genet* 101(3):384.
30. Lima WF*, et al.* (2003) Human RNase H1 activity is regulated by a unique redox switch formed between adjacent cysteines. *J Biol Chem* 278(17):14906-14912.
31. Pettijohn DE & Hecht R (1974) RNA molecules bound to the folded bacterial genome stabilize DNA folds and segregate domains of supercoiling. *Cold Spring Harbor symposia on quantitative biology* 38:31-41.
32. Kruse T*, et al.* (2006) Actin homolog MreB and RNA polymerase interact and are both required for chromosome segregation in Escherichia coli. *Genes Dev* 20(1):113-124.

33. Bestwick ML & Shadel GS (2013) Accessorizing the human mitochondrial transcription machinery. *Trends Biochem Sci* 38(6):283-291.
34. Santamaria D*, et al.* (1998) DnaB helicase is unable to dissociate RNA-DNA hybrids. Its implication in the polar pausing of replication forks at ColE1 origins. *J Biol Chem* 273(50):33386-33396.
35. Terzioglu M*, et al.* (2013) MTERF1 binds mtDNA to prevent transcriptional interference at the light-strand promoter but is dispensable for rRNA gene transcription regulation. *Cell Metab* 17(4):618-626.
36. Fan L, Sanschagrin PC, Kaguni LS, & Kuhn LA (1999) The accessory subunit of mtDNA polymerase shares structural homology with aminoacyl-tRNA synthetases: implications for a dual role as a primer recognition factor and processivity clamp. *Proc Natl Acad Sci U S A* 96(17):9527-9532.
37. Spelbrink JN*, et al.* (2001) Human mitochondrial DNA deletions associated with mutations in the gene encoding Twinkle, a phage T7 gene 4-like protein localized in mitochondria. *Nature Genet* 28(3):223-231.
38. Kornblum C*, et al.* (2013) Loss-of-function mutations in MGME1 impair mtDNA replication and cause multisystemic mitochondrial disease. *Nature Genet* 45(2):214-219.
39. Almalki A*, et al.* (2014) Mutation of the human mitochondrial phenylalanine-tRNA synthetase causes infantile-onset epilepsy and cytochrome c oxidase deficiency. *Biochim Biophys Acta* 1842(1):56-64.
40. Bonnen PE*, et al.* (2013) Mutations in FBXL4 cause mitochondrial encephalopathy and a disorder of mitochondrial DNA maintenance. *Am J Hum Genet* 93(3):471-481.
41. Van Goethem G, Dermaut B, Lofgren A, Martin JJ, & Van Broeckhoven C (2001) Mutation of POLG is associated with progressive external ophthalmoplegia characterized by mtDNA deletions. *Nature genetics* 28(3):211-212.
42. Dalla Rosa I*, et al.* (2016) MPV17 Loss Causes Deoxynucleotide Insufficiency and Slow DNA Replication in Mitochondria. *PLoS genetics* 12(1):e1005779.
43. Saada A (2004) Deoxyribonucleotides and disorders of mitochondrial DNA integrity. *DNA and cell biology* 23(12):797-806.
44. Dalla Rosa I*, et al.* (2014) MPV17L2 is required for ribosome assembly in mitochondria. *Nucleic Acids Res* 42(13):8500-8515.
45. Reyes A*, et al.* (2011) Actin and myosin contribute to mammalian mitochondrial DNA maintenance. *Nucleic Acids Res* 39(12):5098-5108.
46. Brody JR & Kern SE (2004) Sodium boric acid: a Tris-free, cooler conductive medium for DNA electrophoresis. *BioTechniques* 36(2):214-216.

Figure Legends

Figure 1. Many molecules of murine mitochondrial DNA contain a mitochondrial R-loop complementary to the 7S DNA of the mitochondrial D-loop. (**A**) Purified mouse mtDNA (See *SI Appendix* Fig. S2) was digested with Bcl1 and fractionated by 2D-AGE, prior to gel-extraction of the material close to the base of the initiation arc (circled on a representative blot, hybridized to probe np 15551-16034). Repeated 2D-AGE of the gel-extracted nucleic acids confirmed that the majority was more massive than the linear restriction fragment; and heat denaturation and repeated 1D-AGE of samples, untreated (U), treated with RNase HI (R) or DNase (D) as previously (18), revealed an L-strand RNA complementary to 7S DNA. (**B**) A double digest of mouse mtDNA to create a smaller CR-containing fragment reveals two discrete species (**D** and **R**) well separated from the linear 1.35 kb fragment. **C)** 2D-AGE of BseR1 digested mouse mtDNA and enzyme treatments indicate species **R** is more sensitive to Eco-RNase HI than **D**, whereas both are largely resistant to RNase T_1.

Figure 2. Mapping of the mouse mitochondrial R-loop. RNAs recovered from Bcl1 digested mouse liver mtDNA fractionated by 2D-AGE, see Fig. 1A and main text), or undigested purified mouse liver mtDNA, were DNase-treated, circularized, converted to DNA by RT-PCR, cloned and sequenced. The lengths of the R-loops (red lines) are inferred from the junctions (see *SI Appendix*, Table S1) and are aligned to the control region of murine mtDNA. Circularized RT-PCR applied to purified mouse mt-RNA yielded a small number of clones (red lines in gray box, at the base of the figure); and circularized-PCR, cloning and sequencing was used to map the ends of gel-extracted 7S DNAs (blue lines). LSP – light strand promoter; TAS - Termination Associated Sequence; Thr - tRNA threonine gene; Pro – tRNA proline gene; Ori-b and Ori-H - origins of replication; CSB – conserved sequence block; short black arrows mark the approximate position of the primers used for RT-PCR. A – adenine residues added post-transcriptionally to the 3´ end of the RNAs.

Figure 3. Inter-strand nucleic acid cross-linking stabilizes mitochondrial D-loops and R-loops in human cultured cells, and both are mobility shifted by SSB. A) Human 143B osteosarcoma cells were Psoralen/UV cross-linked or left

untreated (control) and the isolated DNA digested with Sac2 and Dra1 prior to 2D-AGE, and blot hybridization to a probe spanning np 16,341-151 that detects the D-loop region (np 16,107-191). An overlay shows the mobility of species D and R relative to a recognized species on the replication fork arc (Y). Vertical broken blue lines indicate the mobility of various species in the first dimension electrophoresis step that is indicative of their mass. Interpretations of the structures of the nucleic acids appear to the right of the gel images: L or 1n – linear duplex mtDNA fragment; Y – replication fork; D-loop – 1n + 7S DNA; R-loop – 1n + LC-RNA (see text for details). The slower mobility of the R-loop in the second dimension compared to the D-loop might reflect a general feature that distinguishes the two types of triple stranded molecule (i.e. the different properties of molecules with a third strand of RNA as oppose to DNA), or it could be indicative of a more complex arrangement of LC-RNA that includes segments of RNA-RNA pairing, as well as RNA/DNA hybrid. Species D and R of human (**B**) and mouse (**C**) mtDNA are mobility shifted by incubation with SSB. RNase T_1 was applied before SSB incubation to remove any RNA tails that might otherwise have accentuated the mobility shift. The probe for mouse mtDNA spanned np 15,511-16,034. Merged false-color images at the foot of the panel C provide a direct comparison of the effect of SSB on the mobility of D- and R-loops: green, C-i merged with red, C-ii or C-iii.

Figure 4. V142I RNase H1 protein is unstable, but the mutant protein does not appreciably alter mtDNA copy number. (**A**) Quantitative PCR to a fragment of a nuclear and a mitochondrial gene (see *SI Appendix*) was used to determine the relative abundance of mtDNA in V142I RNase H1 fibroblasts (V142I) compared to three control human fibroblast lines (CF); data from 3 independent experiments are represented as the mean ± SEM. Inset a representative immunoblot for TFAM and the the reference protein GAPDH. Immunoblots of proteins from control and patient-derived fibroblasts, stored frozen (**B**) or freshly prepared **(C).** RNase H1, MGME1, a mitochondrial endonuclease (Atlas), and vinculin, a reference protein. Proteins were fractionated by 4-12% SDS-PAGE.

Figure 5. 7S DNA molecules are persistently attached to their primer RNA in murine cells lacking RNase H1, but there is no evidence of primer retention in human cells with V142I RNase H1. (**A**) MEF mtDNA, from cells treated for 8 days

without (control) or with 4HT to excise the *Rnaseh1* gene (ΔRH1), was digested with Dra1, left untreated (U) or treated with DNase (D) or Eco-RNase HI (RH); denatured in 80% formamide, 15 min at 85ºC, and separated by 1D-AGE (1% Tris-borate). λ-Hind3 DNA ladder was run in parallel to provide size markers. Southern hybridization with a riboprobe to the 5´ end of the H-strand (H15511-16034) detected the full length H-strand of 3.6 kb (1n) and nascent strands (ns) (described in detail in (15)) and 7S DNA. 7S DNA without a primer is not detected by m-H16051-161832, but is detected by m-H15511-16034 (albeit only in ΔRH1 samples). Line drawings appear to the right of the gel image to denote 7S DNA with and without an RNA primer; red line, RNA; blue lines, DNA. 7S DNAs of the human mitochondrial D-loop range from ~560-650 nt in HEK cells (**B**) and lack a RNA primer in human cells with wild-type (control) or mutant (V142I) RNase H1. (**C**). Sucrose-gradient purified mtDNAs of HEK cells and fibroblasts were separated by 1D-AGE (2% agarose, sodium borate (46)), after treatment with (+) or without (-) Eco-RNase HI, and denaturation in 80% formamide, 15 min at 85ºC, and hybridized with a riboprobe complementary to nt 15869-168 of human H-strand mtDNA. The mtDNA was run in parallel with a series of markers of defined length (see *SI Appendix*). DNA was extracted from whole 143B cells after 6 days of siRNA (non target – NT, or targeting RNASEH1) (**D**), and from control (CF) or patient-derived (PF) fibroblasts (**E**). (**D** and **E**) DNA was digested with Msc1 and fractionated by 1D-AGE (1%, TAE) and blot hybridized to the indicated probe. Cells were subjected to UV/psoralen cross-linking prior to nucleic acids isolation, and Msc1 and RNase HI (RH) digestions, as indicated. The composition of the 8 and 11 kb species are interpreted in the line drawings, the 11 kb band has a blocked site at np 323 owing to the R-loop; RNA, red line, black lines, DNA.

Figure 6. V142I RNase H1 has opposite effects on the abundance of mitochondrial D-loops and R-loops. (**A**) Whole cell DNA from control (C) and V142I RNase H1 (P) fibroblasts was denatured in 80% formamide, 15 min at 85ºC and fractionated by 1D-AGE, where indicated samples were digested with Bsu361 or Xho1. After blot transfer, nascent H-strands and 7S DNA were detected by hybridization to probe h-H15869-168. (**B**) Equivalent DNA samples were denatured after digestion with BsaW1 to shorten the nascent strands and allow higher-resolution mapping on 2% agarose, sodium borate gels (15, 46), (nascent strands with retained primers would resolve above the np 323 marker, see *SI Appendix*, Fig. S6C). (**C**)

Ban2 and Acc1 digested whole cell DNAs of control (C) HEK cells, or cells expressing Twinkle DNA helicase (Twinkle), and from control (C) or V142I RNase H1 (V142I) fibroblasts, were subjected to 1% agarose, 1D-AGE and blot hybridized to h-H15869-168. HEK cell DNA was psoralen/UV cross-linked prior to extraction (see *SI Appendix*).

Figure 7. V142I RNase H1 causes mtDNA aggregation and disruption of mitochondrial morphology. Confocal single optical images of primary human fibroblasts of a control and the index case with V142I RNase H1 were labeled with antibodies to DNA (green), the outer mitochondrial membrane protein, TOM20; the mitochondrial ribosomal proteins MRPS18b or MRPL45 (red) as indicated (**A-C**). DNA in the mitochondria produces co-localization of green and red (yellow). In some cases nuclear DNA was stained (blue) with DAPI. White arrows point to the mtDNA clusters observed in the patient-derived cells (**A**, **D**). (**B**) panel i is a raw confocal optical section of a region of a V142I patient fibroblast depicting antibody staining against mtDNA (green); ii is the reconstruction of i treated with a custom deconvolution algorithm to extend the resolution, and showing that the large mtDNA foci comprise multiple smaller units of similar sized particles. Such particles colocalize (yellow) with staining for antibodies against the mitochondrial ribosomal subunits MRPS18b and MRPL45, and the outer mitochondrial membrane protein TOM20 (**C**). (**D**) Single confocal optical section of V142I RNaseH1 and control fibroblasts treated with 20 μM BrdU. Replicating DNA is visualized with antibodies against BrdU (green), and mitochondria with anti-Tom20 (red), cell nuclei are stained with DAPI (blue). Images show clustering of BrdU signal in V142I RNaseH1 patient fibroblast cells similar to the DNA clusters in other panels, and Fig. S3. White horizontal bars represent a width of 20 μm (**A** and **D**) or 5 μm (**C**).

Figure 8. V142I RNase H1 quiescent cells and muscle display mtDNA aggregation. Confocal optical images of quiescent human fibroblasts (**A**) and a 12 μm transverse section of muscle (**B**) of controls and the index case with V142I RNase H1. Samples were labeled with antibodies to DNA (green), the outer mitochondrial membrane protein, TOM20 (red), and stained with DAPI (magenta). White arrows and zoomed images highlight some of the mtDNA clusters observed in the patient-derived

cells that stained with DAPI. (**B**) Tom20, DNA merged images; for individual components and DAPI staining, and additional muscle fibers see *SI Appendix*, Fig. S10.

Fig. 9. V142I RNase H1 impairs mitochondrial translation and respiration. (**A**) One-hour ^{35}S-methionine labeling of nascent mitochondrial polypeptides in control (CF) or V142I RNase H1 patient (PF) fibroblasts, fractionated by 12% SDS-PAGE. To the left of the gel tentative polypeptide assignments are ND1-6, cyt b, COX1-3 and A6, A8: subunits of respiratory chain complexes I, III and IV, and ATP synthase, respectively. The panel shows two of four experiments, the pair of samples to the right derived from cells grown to full confluence. V142I cells displayed a 34% decrease in mitochondrial translation compared to the two control cell lines analyzed, based on quantitation of the indicated bands (*). (**B**) Mitochondrial oxygen consumption rate (OCR) was measured using a Seahorse flux analyzer before (basal) and after the addition of uncoupler FCCP (maximal), having subtracted the non-mitochondrial (rotenone-insensitive) OCR. The data represent the mean ± SEM of 4 independent experiments, each one performed in duplicate. Statistical analysis was performed using an unpaired two-tailed Student's t-test. Maximal respiration of the V142I (P) cells was significantly lower than the controls (C) $p = 0.018$.

Supporting Information

Materials and Methods

Patients: Exome sequencing identified homozygous missense mutations in *RNASEH1*, c.424G>A; p.Val142Ile (V142I), in the affected members of two unrelated families with neuromuscular disease. All unaffected members of the families had at least one normal allele. In Family 1, the two affected siblings developed ptosis, chronic progressive external ophthalmoplegia, ataxia, proximal myopathy and a sensorimotor neuropathy in adult life; a very similar clinical phenotype was exhibited by the four affected siblings of Family 2. The muscle tissue of all affected individuals in both families manifested multiple mtDNA deletions and frequent cytochrome *c* oxidase and ragged red fibers (Fig. S5). The patient derived fibroblasts used in the study were from family 2 member III-9 (Fig. S5A).

Mitochondrial DNA preparation from solid tissue: Ten grams of finely chopped mouse liver was suspended in 9 vol homogenization buffer (HB)/g liver and subjected to 3 strokes of Dounce homogenization with a tight fitting pestle. HB is 225 mM Mannitol, 75 mM Sucrose, 2 mM EDTA and 10 mM HEPES-NaOH (pH 7.6). The homogenate was centrifuged at 600 g_{max} for 10 min, and the supernatant re-centrifuged at 7,000 g_{max} for 10 min to obtain a crude mitochondrial pellet. The mitochondrial pellet was re-suspended in 5 vol HB/g liver, centrifuged at 7,000 g_{max} for 10 min, and this step was repeated with 2.5 vol HB/g liver. The second mitochondrial pellet was re-suspended in 0.5 vol HB/g liver and loaded on to a 1M/1.5M sucrose step-gradient, in 2 mM EDTA and 10 mM HEPES-NaOH (pH 7.8), and centrifuged at 40,000 g_{max} for 1 h. The mitochondrial layer was diluted to 250 mM sucrose, 2 mM EDTA and 10 mM HEPES pH 7.8 and sedimented by centrifugation at 9,850 g_{max} for 10 min. The mitochondrial pellet was re-suspended in 75 mM NaCl, 50 mM EDTA, 20 mM HEPES pH 7.2 and divided into 4 equal fractions (of ~10 mg) (a-d, see Fig. S2). All the above procedures were performed on ice in a cold-room. Mitochondria were incubated with 100 μg/ml Proteinase K on ice for either 45 min (A-C) or 10 min (D). Next the mitochondria were lysed with 1% sodium N-lauroylsarcosinate (sarcosine) and incubated at 50^{o}C for 45 min (a) 10 min (b), or 0 min (c and d) (Fig. S2); and the nucleic acids isolated by successive phenol and chloroform extractions, followed by 2-propanol precipitation. All chemicals used were RNase- and DNase-free grade. For

all the subsequent R-loop analysis the 50ºC step was omitted and Proteinase K treatments were performed on ice for 10-45 mins.

Cell culture and mitochondrial DNA isolation: Proliferating human cells were cultured in Dulbecco's Modified Eagle's Medium (DMEM), with 10% fetal bovine serum. Cells were harvested in PBS and mtDNA extracted as previously (1). For whole cell DNA isolation, cells were lysed in HB. After cell or mitochondrial lysis with 0.25% sodium sarcosine and digestion with 1 mg proteinase K per 5 x 10^6 cells for 1-6 h at 37ºC, nucleic acids were isolated via phenol-chloroform extraction, and precipitated with 0.1 vol of 3M sodium acetate and 0.8 vol 2-propanol; DNA was recovered by centrifugation, re-suspended in 10 mM Tris pH 8.0 and stored at -20°C. For nucleic acids cross-linking, cells were pre-incubated in 10 μM 4,5',8-trimethylpsoralen (TMP) for 10 min at 37ºC and exposed to 365 nm UV light for a further 10 min at room temperature. The cells were washed once in PBS and lysed immediately to extract DNA as above. Quiescence was induced in the fibroblasts by reducing the serum concentration of the growth medium from 10% to 0.1% and the cells analyzed 10 days later.

Nucleic acid digestion, modification and analysis: Restriction digestions of 2-10 μg of whole cellular DNA, or 2-4 μg lots of DNA from purified mitochondria, were performed in 40-200 μl volumes according to the manufacturer's instructions, and then precipitated with ethanol and salt and re-suspended in 10 mM Tris pH 8.0. Where indicated samples were treated additionally with 1 U of E. coli RNase HI (Promega or Takara) for 15-60 min at 37°C. Incubation with recombinant SSB from E. coli (Promega) was as previously (2). Denaturation of DNA was achieved by mixing with an equal volume of formamide, heating to 95°C for 5 min and quenching on ice for 2 min. DNA was fractionated in one dimension (1D-AGE) either on 0.8-1.5% Tris-acetate agarose (Invitrogen) gels overnight at 0.8 V/cm or 2-2.5% Nu-Sieve 3:1 agarose (Lonza) gels (10 mM sodium borate), at 17.5 V/cm for 4-6 h at room temperature with circulation. Two dimensional agarose gel electrophoresis was as previously described (3). After electrophoresis, gels were soaked for 30 min in 5 x SSC and 10 mM NaOH and then transferred to nylon membrane overnight by capillary transfer using 5 x SSC, 10-100 mM NaOH. DNA was cross-linked to the membrane by exposure to UV at 1200 μJ/cm. Membranes were then probed with radiolabeled DNA, prepared using a random-prime labeling kit (GE Healthcare); or riboprobes, using T7-

maxiscript kit (Ambion) as per the manufacturer's instructions. Probing of the membrane was performed overnight at 55-60°C in 2 x SSPE, 2% Sodium dodecyl sulfate, 5 x Denhardts Reagent, 5% Dextran sulfate buffer. After overnight incubation, membranes were washed four to six times with 0.1-1 x SSPE, 0.5% SDS, at 55°C. Membranes were exposed to X-ray film or phosphorscreens for 4-120 h and imaged on a Typhoon scanner (GE Healthcare). Image J software was used to quantify D-loop and R-loop levels.

Detection and characterization of the mitochondrial R-loop: To determine the composition of small bubble-like structures associated with fragments of mtDNA containing the control region, BclI digested mouse liver mtDNA was fractionated by 2D-AGE and the portion of the gel running slightly above the linear 4.15 kb fragment (np 12,034-16,179) was excised and the nucleic acids recovered by electrophoresis into dialysis tubing. Some gel-extracted material was treated with RNase HI, DNase or no enzyme, prior to denaturation and re-fractionated by 1D-AGE, as previously applied to mtDNA replication intermediates (3). The products were re-fractionated by 1D-AGE and hybridized to H- and L-strand specific riboprobes generated from amplified mouse (m) mtDNA with the following primers (5′-3′, with the T7 promoter sequence underlined.): TAATACGACTCACTATAGGCAATGGTTCAGGTCATAAAA TA ATCATC, m-H15,511-15,539 and GCCTTAGGTGATTGGGTTTTGC m-H16,034-16,012; CAATGGTTCAGG TCATAAAATAATCATC, m-L15,511-15,539 and TAATA CGACTCACTATAGGGCCTTAGGTGATTGGGTTTTGC m-L16,034-16,012.

For sequencing, gel-extracted material, or purified mtDNA was treated with 2 U Turbo DNase I (Ambion) in 20 µl at 37°C for 1 h; incubated with 20 U T4 RNA ligase in 1 x RNA ligase buffer, 12% PEG 6000 to circularize the RNA. For reverse transcription the RNA was incubated with 0.5 mM dNTPs, 0.5 µM primer R1 (m-L15,897-15,918 GTGGTGTCATGC ATTTGGTATC), 4 U Omniscript reverse transcriptase in 1 x RT buffer, in 20 µl at 37°C for 1 h. For PCR across the ligation junctions to identify the ends of the RNAs, the DNA was amplified using 1U Vent polymerase in 50 µl of 1 x amplification buffer, 0.1 µM primer F1 (m-H15,840-15,821 GGGAACGTATG GGCGATAAC) and R1, 0.25 mM dNTPs for 35 cycles of 95°C 2 min, 56°C 1 min, 76°C 1 min, and an elongation step of 10 min at 76°C. 2-5 µl of the PCR reaction served as template in a second amplification reaction comprising template, 3U BioTaq, 1 x BioTaq buffer, 1.5 mM $MgCl_2$, 0.12 µM primers F2 (m-H15,704-15,680

CACGGAGGATGGTAGATTAATAGA) and R2 (mH-15,949-15,969 GCCGTCAAG GCATGAAAGGAC), 0.3 mM dNTPs in 50 µl. Reaction conditions were 95°C for 3 min followed by 35 cycles of 95°C 0.5 min, 58°C 0.5 min, 72°C 0.5 min, and an extension step of 72°C for 10 min. The products were gel-extracted (QIAquick Gel Extraction Kit) and cloned into PCR2.1 vector using 50 ng of vector, 4U T4 DNA ligase in 1 x DNA ligase buffer for 14 h at 14°C. The ligated DNA was transformed into Top10 E. coli and clones carrying a DNA insert sequenced commercially. On one occasion the same procedure was applied to Trizol™ purified RNA from purified mouse liver mitochondria; and the ends of 7S DNAs were determined using the same primers and purified mtDNA, omitting the DNase treatment and reverse transcription steps.

Additional Primer pairs for hybridization probes:

Mouse

m-14903-15401: 5´-CAGACAACTACATACCAGCTAATCCAC and 5´-ACCAGCTTTG GGTGCTGGTG. m-15511-16034: 5´-ATCAATGGTTCAGGTCATAAAATAATCATCA AC-3´ and 5´-GCCTTAGGTGATTGGGTTTTGC-3´. m-H16051-16183: 5´-TAATAC GACTCACTATAGGGTTAGACATAAATGCTACTCAATACC-3´ and 5´-GATCAGGAC ATAGGGTTTGATAG-3´.

Human (h)

h-H15,869-168: 5´-TAATACGACTCACTATAGGAAAATACTCAAATGGGCCTGTCC-3´ and 5´-GGTGCGATAAATAATAGGATGAGG-3´. h-16,341-151: 5´-TTACAGTCAA ATCCCTTCTCGTCC-3´ and 5´-GGATGAGGCAGGAATCAAAGACAG-3´.

Q-PCR of human mtDNA: MtDNA was quantified as described in (4). Briefly, total DNA was isolated from human fibroblasts using DNeasy Blood and tissues Kit (QIAGEN). 25 ng DNA were used as template for amplification of COXII gene in a real-time quantitative PCR reaction (7550 Fast Real-Time PCR, Applied Biosystem). A portion of APP1 gene was amplified simultaneously as nuclear reference. Primers: hCOXII: 5´-CGTCTGAACTATCCTGCCCG-3´ and 5´-TGGTAAGGGAGGGATCGT TG-3´, hAPP-F: 5´-TTTTTGTGTGCTCTCCCAGGTCT, and 5´-TGGTCACTGGTTGG TTGGC-3´.

Immuno-blotting: Protein fractionation, transfer and immuno-detection were performed as described (5), with some modifications. Cells were lysed on ice in PBS, 1% SDS, 1 X protease inhibitors cocktail (Roche) and 50 U Benzonase (Millipore). Protein concentration was measured by Lowry assay (DC™ Reagent, Biorad) and 20 µg of lysates analyzed per lane. For RNAse H1 immunodetection, samples were treated with 2 mM DTT as reducing agent. Primary antibodies employed were: mouse anti-RNase H1 (abcam # 56560, 1:500) and mouse anti-VCL (abcam # 18058, 1:5000).

Primers for markers of defined length: for high-resolution 1D-AGE were generated by PCR amplification of human mtDNA with forward primer: h15869 5´-AAA ATACTCAAATGGGCCTGTCC-3´ and the following series of reverse primers: h-54 5´-CCAAATGCATGGAGAGCTCC-3´; h-111 5´-TGCTCCGGCTCCAGCGTC-3´; h-150 5´-GATGAGGCAGGAATCAAAGACA-3´; h-168 5´-GGTGCGATAAATAATAGG ATGAGG-3´; h-191 5'-TGTTCGCCTGTAATATTGAACG-3´; h-240 5'-TATTA TTATGTCCTACAAGCAT-3´; h-300 5'-TGGTGGAAATTTTTTGTTATGATG-3'; h-407 5'-AAAGATAAAATTTGAAATCTGGT-3'. PCR products were digested with Dra1 to create a consistent end at np 16,010 prior to 1D-AGE fractionation of the markers. Another marker spanning the BsaW1 site at np 15,924 to 50 was generated by digesting 143B crude mtDNA with BsaW1 and BstX1 to create a product of 699 bases in length (see Fig 5C).

PCR Conditions: Unless specified elsewhere in the methods, 50 ng of template DNA was incubated with 200 µM of each of the 4 dNTPs, 1.25 U of EX-Taq DNA Polymerase (Takara) in 50 µl of 1 X reaction buffer (Takara), for 30 cycles of 94°C, 30 sec; Tm °C (lower of the 2 primers), 30 sec; 72°C, 30 sec. The 30 cycles were preceded by denaturation for 3 min at 94°C, and followed by a 5 min incubation at 72°C.

Northern Hybridization RNA was extracted from fibroblasts using Trizol according to the manufacturers instructions. Three microgram aliquots were fractionated on 1% agarose gels in 1 x MOPS buffer, and blot hybridized to radiolabeled probes derived from regions of mtDNA amplified with primers 5'-CACCCAACAATGACTAATC AAACTAACCTC-3´ and 5´-TATGAGGAGCGTTATGGAGTGGAAG-3´ (A6/A8); 5´-TATTCCTAGAACCAGGCGACCTGC-3´ and 5´-TTTCGTTCATTTTGGTTCTCAGGG

TTTG-3´ (COX2); and 5´-CTGCCATCAAGTATTTCCTCACGC-3´ and 5´-TCAGGTGCGAGATAGTAGTAGGGTC-3 (ND2).

Gene-silencing of RNase H1: RNA interference of RNase H1 in human 143B osteosarcoma cells was as described (6). Briefly, 2 x 10^6 143B cells were transfected with lipofectamine RNAiMAX (Invitrogen) combined with 10 nM dsRNA [5´-GGAUGGAGAUGGACAUGAAAG-3´, 5´-UUCAUGUCCAUCUCCAUCCAG-3´] according to the manufacturer's instructions. The same number of cells was re-transfected 72 h after the first transfection and the nucleic acids harvested 72 h later. Repression of the target protein after siRNA was confirmed by immunoblotting.

Immunocytochemistry: Patient and control fibroblast cultures, the cells were incubated with 20 µM BrdU for 10 h and fixed with 2% paraformaldehyde 15 min at room temperature, treated with phosphate buffered saline (PBS) containing 0.2% Triton X-100. After a 5 min PBS wash, cells were incubated for 90 min at 40℃ in 2N hydrochloric acid (HCl). 5% goat serum in PBS was applied for 1 h, for blocking, after which the cells were incubated with primary antibody in PBS at 4℃ overnight and subsequently with secondary antibodies for 2 h at ambient temperature. A 90 min incubation at room temperature with Alexa Fluor 488 conjugated streptavidin (Invitrogen) was followed by three PBS washes. The coverslips were mounted on glass slides using Progold with DAPI. For staining which did not include BrdU the HCl antigen retrieval step was omitted. Primary antibodies: mouse anti-DNA Progen (AC-30-10) at 1:200; rat anti-BrdU Bio-Rad (MCA2060) 1:200; rabbit anti-MRPL45 (Proteintech) 1:200; rabbit anti-MRPS18b (Proteintech) 1:200; rabbit anti Tom20 (Santa Cruz) 1:400. Secondary antibodies: Alexafluor 488 goat anti-mouse (1:500); Alexafluor 488 goat anti-rat (1:500); Alexafluor 568 goat anti-rabbit (1:1000).

[^{35}S]-methionine labeling of mitochondrial proteins: mitochondrial translation products in cultured cells were labeled as described previously (5). Fibroblasts were washed twice with methionine/cysteine-free DMEM (Sigma) supplemented with 2 mM L-glutamine, 96 µg/ml cysteine and 5% (v/v) dialyzed FBS followed by a 10 min incubation in this medium at 37^{o}C. Cytosolic translation was inhibited by incubating the cells for 20 min with 100 µg/ml emetine dihydrochloride (Sigma) at 37^{o}C. 100 µCi [^{35}S]-methionine was added to the medium and the cells incubated for 1 h at 37^{o}C, washed three times with PBS and lysed in 1 X PBS, 0.1% n-dodecyl-D-maltoside

(DDM), 1% SDS, 50 U benzonase (Novagen), 1:50 (v/v) protease inhibitor cocktail (Roche). 20 µg lots of protein were fractionated by SDS-PAGE (Novex) and radiolabeled proteins detected by Phosphorimager after drying (Typhoon Molecular Imager FX, GE Healthcare), and quantified using Image J software.

Cellular Oxygen Consumption: The Oxygen Consumption rate (OCR) of adherent fibroblasts was assayed with a XF24 Extracellular Flux Analyzer (Seahorse Bioscience). Briefly, $4x10^4$ proliferating fibroblasts were seeded in microplates (Seahorse Bioscience) in 250 µl of prewarmed growth medium (DMEM, GIBCO) and incubated 37ºC /5% CO_2 for 6 h. Subsequently, the medium was removed and replaced with assay medium and the cells incubated for 30 min in a 37ºC non-CO_2 incubator. After taking an OCR baseline measurement, 1 µM oligomycin, 1.2 µM carbonylcyanide-4-trifluorometho-xyphenylhydrazone (FCCP) and 1 µM rotenone were added sequentially. For normalization, protein concentration in each well was determined using the Lowry assay (Biorad).

Generation of a cell line carrying inducible transgenic TWINKLE: A cDNA of TWINKLE was cloned into vector pcDNA5/FRT/TO (Invitrogen). HEK293T cells (Invitrogen) were transfected with 0.2 µg of pcDNA5.Twinkle and 1 µg of pOG44, using lipofectamine2000 (Invitrogen) according to the manufacturer's instructions. Prior to transfection HEK293T cells were cultured in DMEM supplemented with 10% tetracycline-free fetal bovine serum, 15 µg/ml blasticidin and 100 µg/ml zeocin. Transformants were grown in 15 µg/ml blasticidin, 100 µg/ml hygromycin. Transgene expression was induced for 72 h at a dose of 20 ng/mL doxycycline.

Supplemental Tables

5' end	3' end	mtDNA	Incidence	Length (nt)	polyA
15476	16192	ML6-GE	1	716	
15476	16190	ML6	4	714	
15516	16189	ML6	1	673	
15561	16189	ML6	1	628	
15581	16190	ML6	1	609	11
15580	16189	ML6	1	609	
15584	16190	ML6	1	606	
15586	16190	ML6	1	604	13
15593	16190	ML6	1	597	
15595	16190	ML6	2	595	1
15599	16189	ML6	1	590	
15600	16190	ML6	1	590	2
15601	16189	ML6	2	588	
15609	16188	ML2-GE	1	579	
15660	16190	ML6	1	530	11
15671	16097	ML6	1	426	
15648	16091	ML6	1	443	
15620	16087	ML1-GE	1	467	
15607	16084	ML1-GE	1	477	
15476	16072	ML1-GE	1	596	
15659	16067	ML1-GE	1	408	
15606	16046	ML2-GE	5	440	
15475	16039	ML2-GE	1	564	
15745	16039	ML2-GE	1	294	
15478	16031	ML6	1	553	
15628	16007	ML6	1	379	15
15667	15991	ML1-GE	3	324	
15667	15989	ML1-GE	1	322	
15595	15988	ML1-GE	1	393	
15592	15981	ML1-GE	1	389	

Table S1. Cloned sequences of mouse mitochondrial R-loops (LC-RNA), after circularized RT-PCR. 5´ and 3´ ends denote the ends of the RNAs according to the revised reference sequence of murine mtDNA (7). Blue shading - RNAs with a 3´ end mapping to LSP; purple shading - 5´ ends at TAS; green shading - 5´ ends near Ori-b (see text for details). RNAs were derived directly from purified preparations (numbered chronologically (numbers not listed were used in other studies)) of mouse liver (ML) mtDNA or from gel-extracted material (GE) from the region where the mitochondrial R-loop is predicted to migrate. PolyA – the number of adenosine residues at the 3´ end of the RNA that do not match the reference sequence and are therefore inferred to be added post-transcriptionally.

	Family 2, III.9	Family 2, III.10	Family 2, III.11	Family 2, III.8	Family 1, II.8	Family 1, II.6	Family 1, II.1
Status	Affected	Affected	Affected	Affected	Affected	Unaffected	Affected
Unique reads	30293109	23468401	28223264	31470349	30329427	36841048	n/a
% Aligned	0.79	0.78	0.77	0.78	0.78	0.78	n/a
min 10x depth %	0.79	0.70	0.75	0.79	0.77	0.82	n/a
Tot variants	21372	20316	20930	21478	21542	22161	20075
Homozygous variants	8696	8298	8741	8642	8535	8795	7690
Non-syn variants*	4308	4106	4358	4340	4228	4335	3542
Novel variants	47	36	63	61	56	62	17

Table S2. Exome Sequence Data Summary. Summary of all the variants for each patient (affected and unaffected) where exome sequencing was performed. Results from Exome Sequencing of Families 1 and 2 with variants identified. *includes stop, gain, indel and splice variants. **Total shared variants: 1 RNASEH1 V142I.** All three unaffected family members sequenced had at least one wild-type RNASEH1 allele.

Supplemental Figures

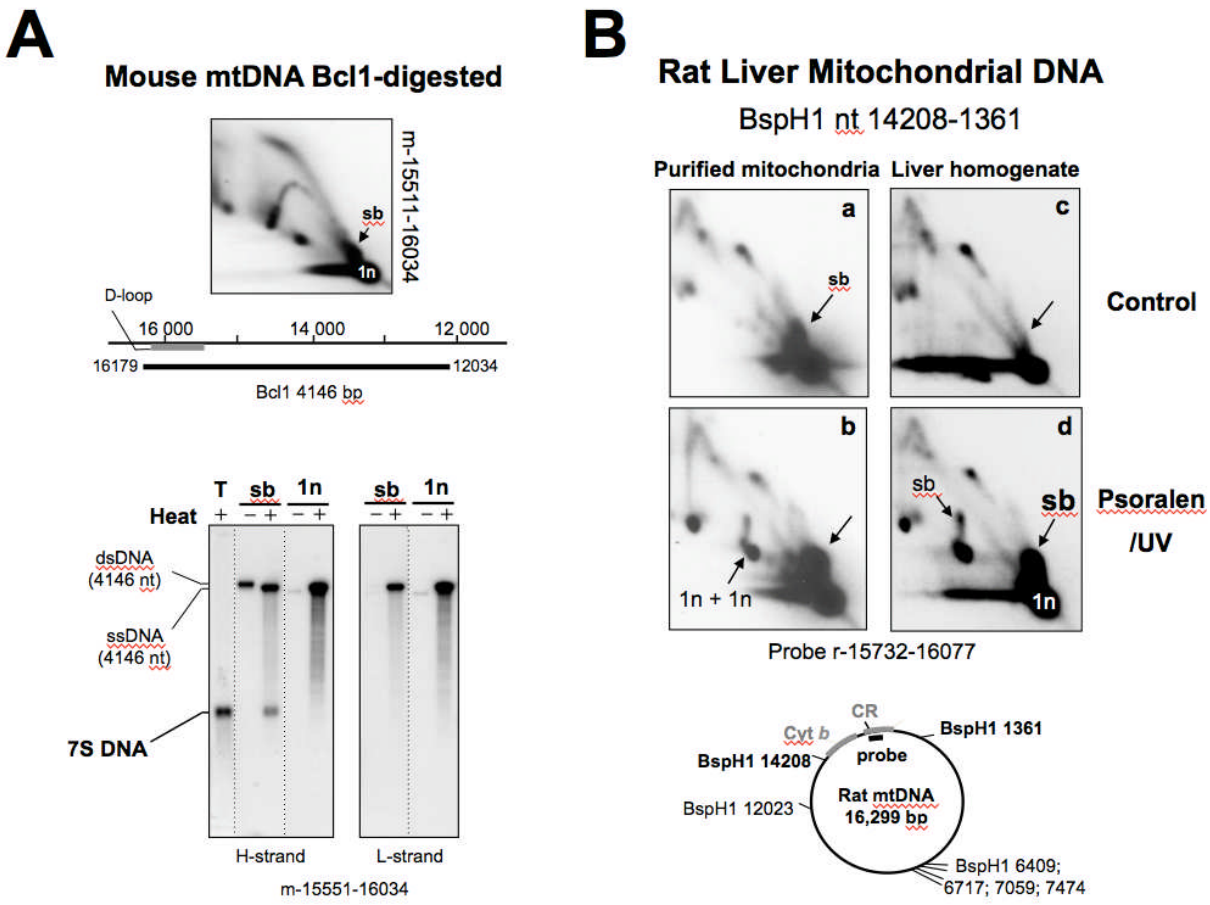

Figure S1. A) In contrast to the new preparations of mouse mtDNA (Fig. 1A), no L-strand nucleic acids species (other than the full-length linear restriction fragment, 1n) were detected when small bubble (sb) structures were gel-purified from the base of an initiation arc, denatured and re-fractionated by 1D-AGE – lower gel image. The L- and H- strand riboprobes for mouse (m) mtDNA spanned np 15,511-16,034. T – total undigested mouse mtDNA. Panel A is adapted from (8). **B**) Psoralen-ultraviolet crosslinking markedly increased the signal (i.e. the stability or integrity) of the small bubble-like structures. DNA from crosslinked (b and d) or control (a and c) rat mitochondria or liver homogenate, digested with BspH1, prior to 2D-AGE and hybridization to a probe spanning np 15,732-16,077 of the Control Region (CR) of rat (r) mtDNA. Crosslinking also prevented cleavage at the np 14,208 BspH1 site in a fraction of molecules producing a new spot (1n [14,208-1,361] + 1n [12,023-14,208]) and an accompanying small bubble (sb) arc. Cyt *b* – cytochrome *b* gene. Panel B is adapted from (9). Based on the new findings reported here the small bubbles comprise D-loops and R-loops in similar amounts.

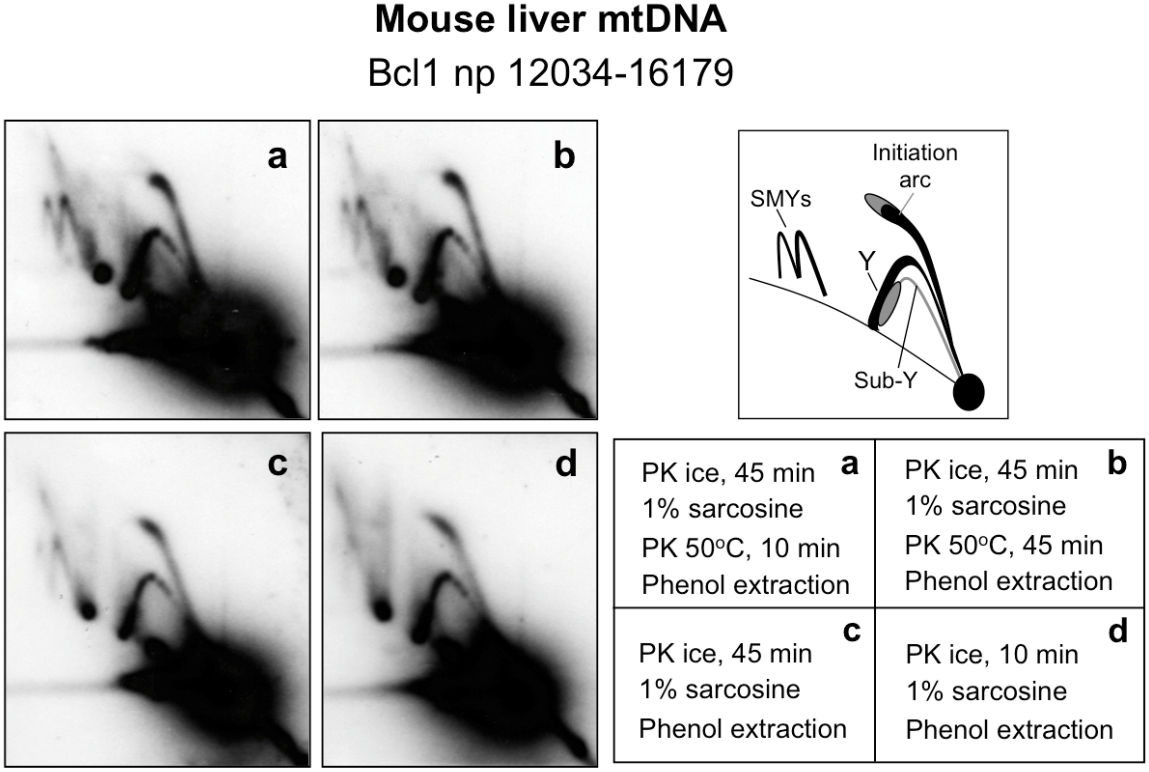

Figure S2. Purification of mouse liver mitochondrial DNA at 4ºC improves the quality of the replication intermediates. Purified mtDNA from mouse liver mitochondria (see methods) were digested with Bcl1 and blot hybridized to probe np 15,551-16,034, after 2D-AGE. Omission of the proteinase K (PK) step at 50ºC after detergent (sarcosine) lysis yielded longer initiation arcs (the final portion indicated in gray in the cartoon), and reduced the signal from the sub-Y arc (again indicated in gray in the cartoon) (panels c and d compared to a and b). 'Retracted' initiation arcs and sub-Y arcs are attributable to the degradation of RNA associated with replicating mtDNA molecules (detailed in (3)). Hence the RNA/DNA hybrids of mtDNA are adjudged to be better preserved using protocols c and d compared to a and b. Therefore, the 50ºC step was avoided for the analysis of RNA/DNA hybrids in the control region of murine liver mtDNA in this report. Y – standard replication fork arc; Sub-Y – partially degraded Y arc, SMYs – slow-moving Y arcs attributable to RNA/DNA hybrids at Bcl1 sites (nps 7,084, 11,329 and 12,034) outside the control region (detailed in (3)).

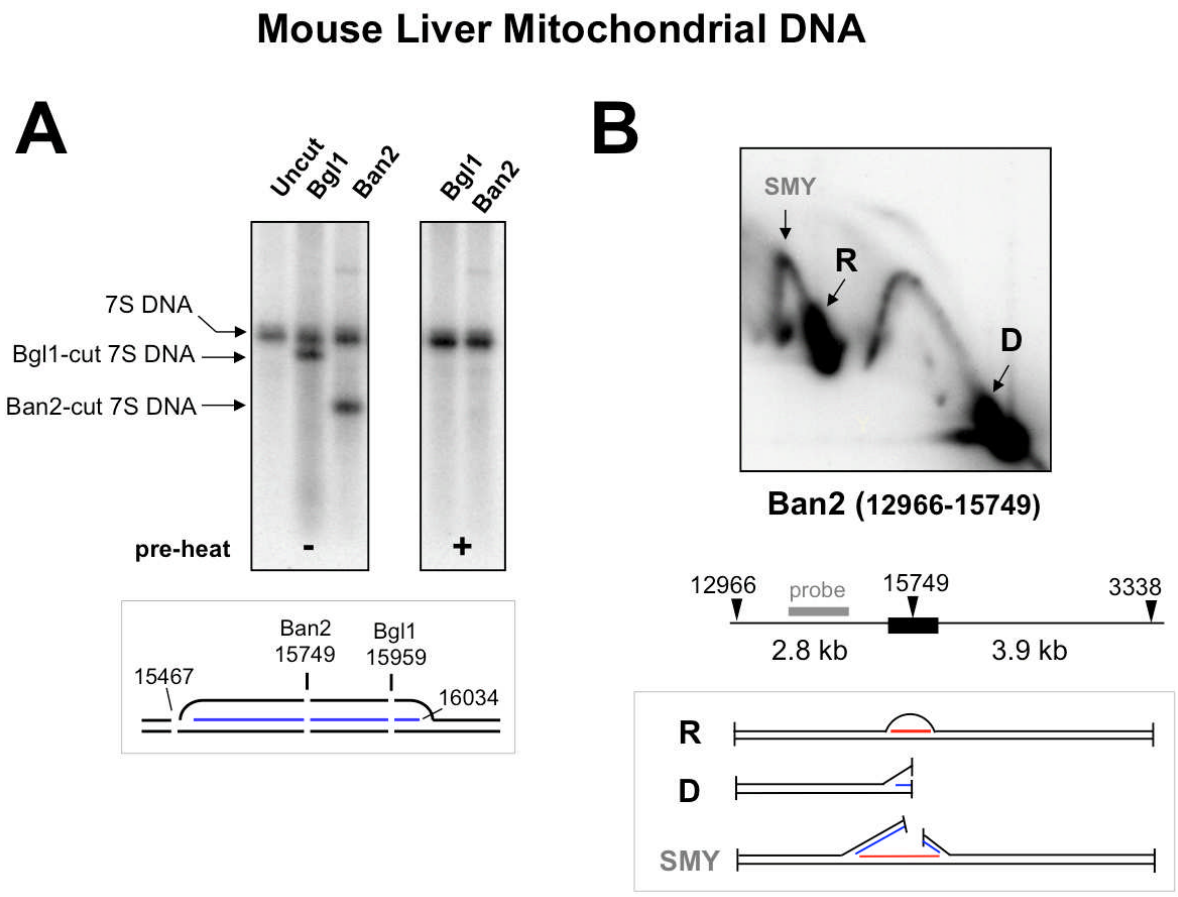

Figure S3. Restriction enzymes, Bgl1 and Ban2 cleave 7S DNA in the form of a D-loop, but not free 7S DNA; they also cut some but not other small bubble structures associated with fragments of mtDNA containing the control region. (**A)** Purified murine liver mtDNA was digested with Bgl1 or Ban2, in one case the samples were pre-heated to 70^{o}C for 15 min to release 7S DNA before loading (preventing cleavage by the restriction enzymes); all were fractionated by 1D-AGE (1% Tris-acetate) and blot hybridized to a probe within the CR (np 15,551-16,034). (**B)** Murine liver mtDNA digested with Ban2 and blot hybridized to probe np 14,903-15,401, after 2D-AGE. Interpretations are shown in the carton: SMYs arising due to RNA/DNA hybrids formed on replicating mtDNA molecules have been described in detail previously (3); R-loops (R) with RNA (red) across np 15,749 prevent Ban2 cleavage at this position, whereas the 7S DNAs of the D-loop (D) (and nascent strands – blue) are cleaved by Ban2.

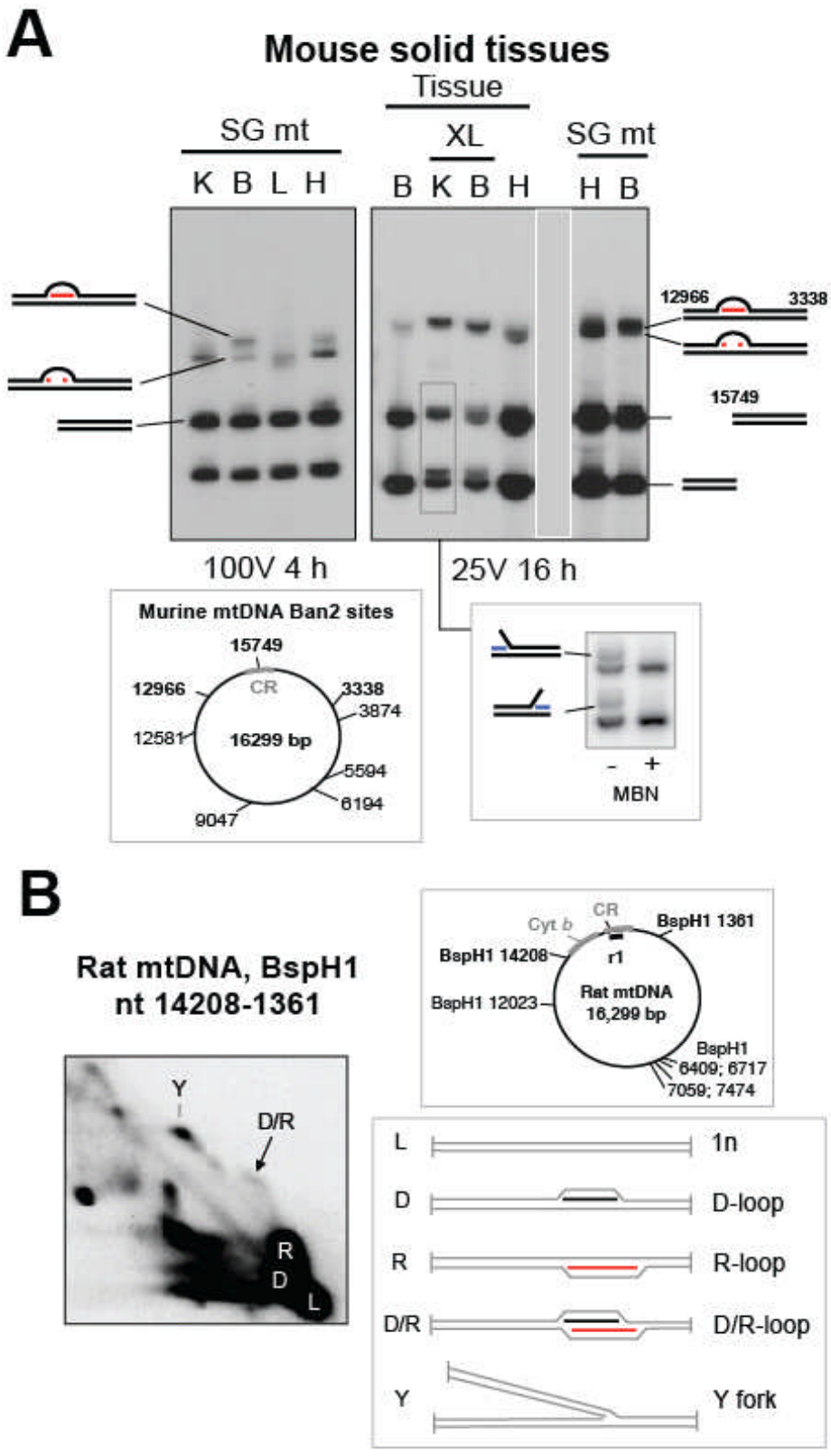

Figure S4. D-loop and R-loop species in mouse and rat tissues. (**A**) Mitochondrial DNA molecules refractive to Ban2 digestion extracted from a variety of mouse tissues. Mitochondrial DNA extracted from sucrose gradient purified mitochondria (SG mt) of B - brain, H - heart, K - kidney or L - liver mitochondria was digested with Ban2 and fractionated by 1D-AGE (1% Tris-borate), blot hybridized to a probe spanning np 15,450-16,034 of the mouse mitochondrial genome. Separately, total tissue DNA was extracted

from murine kidney and brain after dounce homogenization and 10 μM, 10 psoralen/UV cross-linking at 365 nm for 10 min (XL), and subjected to the same Ban2 digestion and fractionation. Interpretations are shown to the sides of the gel images. R - R-loops with RNA in red across np 15,749 prevents Ban2 cleavage at this position, whereas the 7S DNAs (blue), of the D-loop (D), are cleaved by Ban2. A gray box covers one lane that does not add materially to the results. The preparation of liver mitochondria was slower than for the other tissues, which may account for the few surviving R-loops on this occasion in this tissue. The species assigned as D-loop containing fragments were, as expected, modified by mung bean nuclease (MBN) treatment that cleaves single stranded DNA (inset). (**B**) Psoralen/UV crosslinking of rat liver mtDNA yields an arc projecting from the R-loop and D-loop spots that is commensurate with synthesis of a dual D/R-loop. DNA from cross-linked rat mitochondria, digested with BspH1, prior to 2D-AGE and hybridization to a probe to the CR (panel B is adapted from (9)).

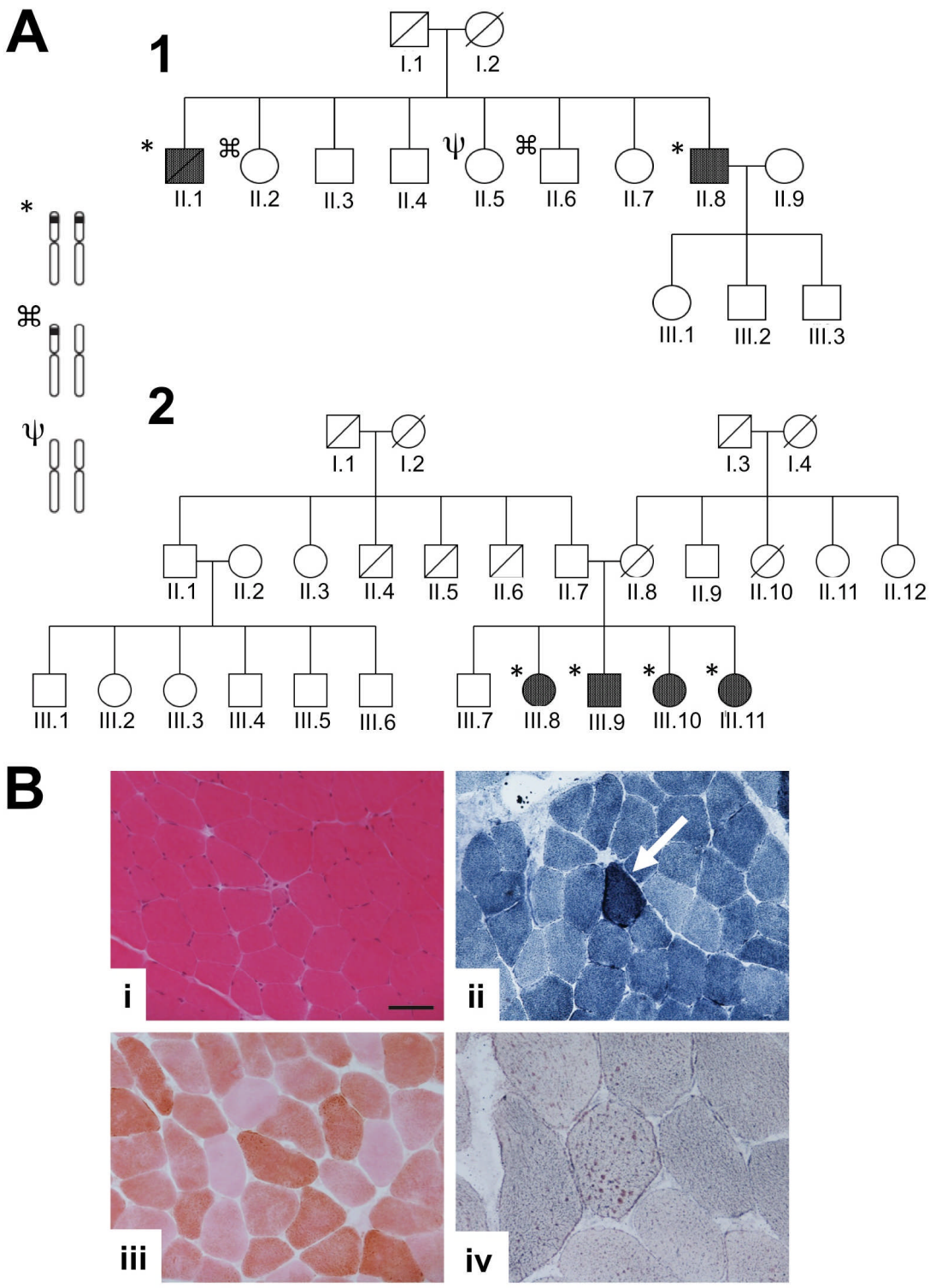

Figure S5. Pedigrees of the two families (1 and 2) with a homozygous missense mutation in RNASEH1, c.424G>A; p.Val142Ile (A) and muscle histochemistry of an affected patient (II-8) (B). Chromosome annotations in panel **A**, ψ-homozygous c.424G, ⁎-homozygous c.424A (V142I), ⌘-heterozygous individuals. Sparse atrophic fibres visualized in Haematoxylin and Eosin preparation (B-i). Succinate dehydrogenase staining revealed ragged red equivalents (white arrow) (B-ii). Histochemical staining for cytochrome c oxidase demonstrated significant numbers of fibres with deficient enzyme activity (B-iii). Sudan black stain showing increased lipid droplets in central fibers (B-iv). Bar represents 50 μm in B-i-iii and 25 μm in B-iv.

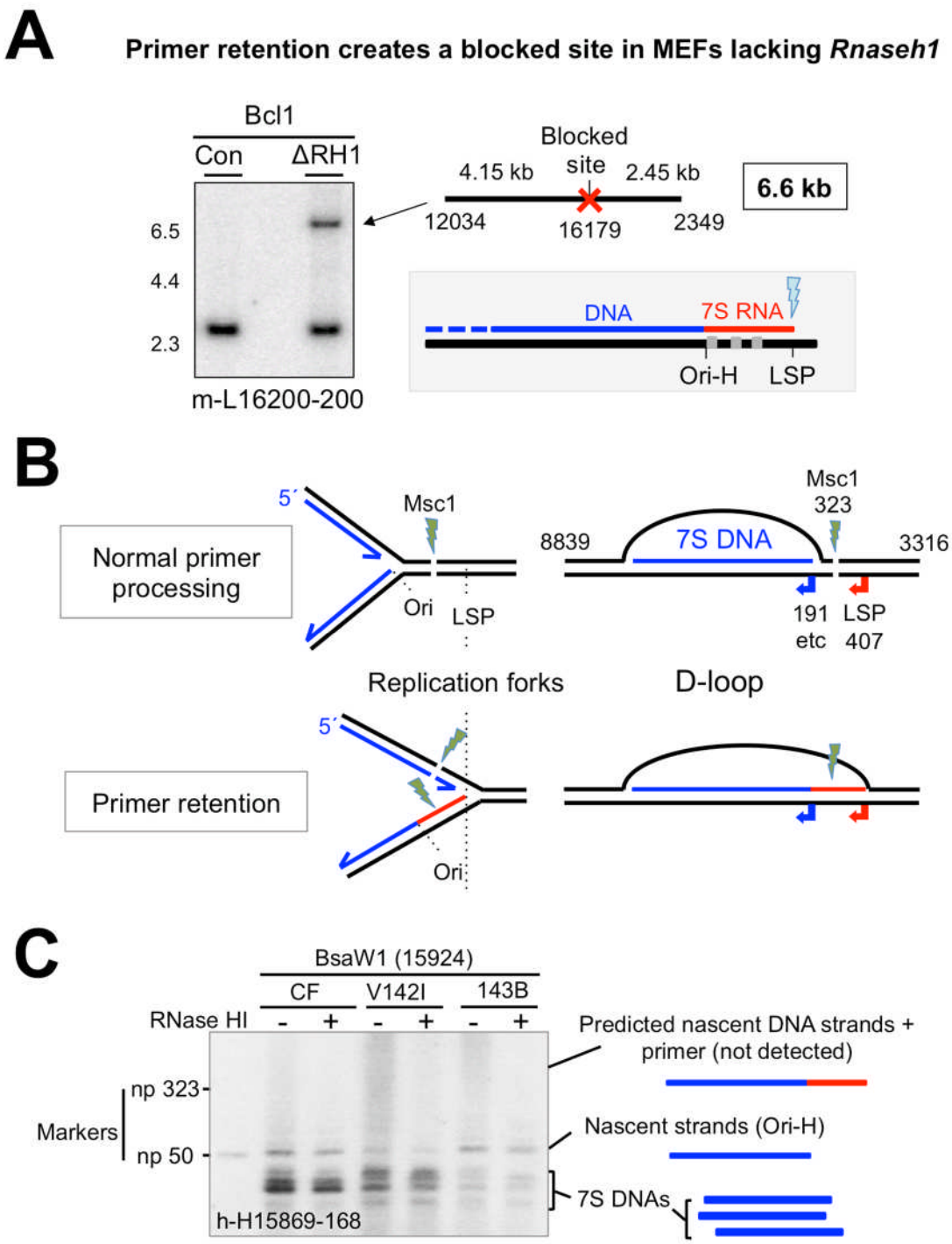

Figure S6. Primer retention generates RNA/DNA hybrids that are refractive to restriction digestion, but primer retention is not evident in V142I RNase H1 fibroblasts. (**A**) An inability to remove the RNA spanning LSP to Ori-H (or Ori-b, not illustrated) in MEFs lacking RNase H1 blocks a restriction site at np 16,179, immediately downstream of LSP (adapted from (15)). (**B**) Likewise, primer retention in human mtDNA will result in failure to cut mtDNA molecules at the np 323 Msc1 site. However, np 323 is cut as normal in cells with V142I RNase H1 (Fig. 5E) and nascent strands and 7S DNAs remain the usual length, with and without in vitro RNase HI treatment (Fig. 6B and panel **C** above). (**C**) DNA from V142I and control fibroblasts and 143B cells was BsaW1

digested, denatured, fractionated and probed as per Fig. 6B, additionally some samples were treated (+) with *E. coli* RNase HI.

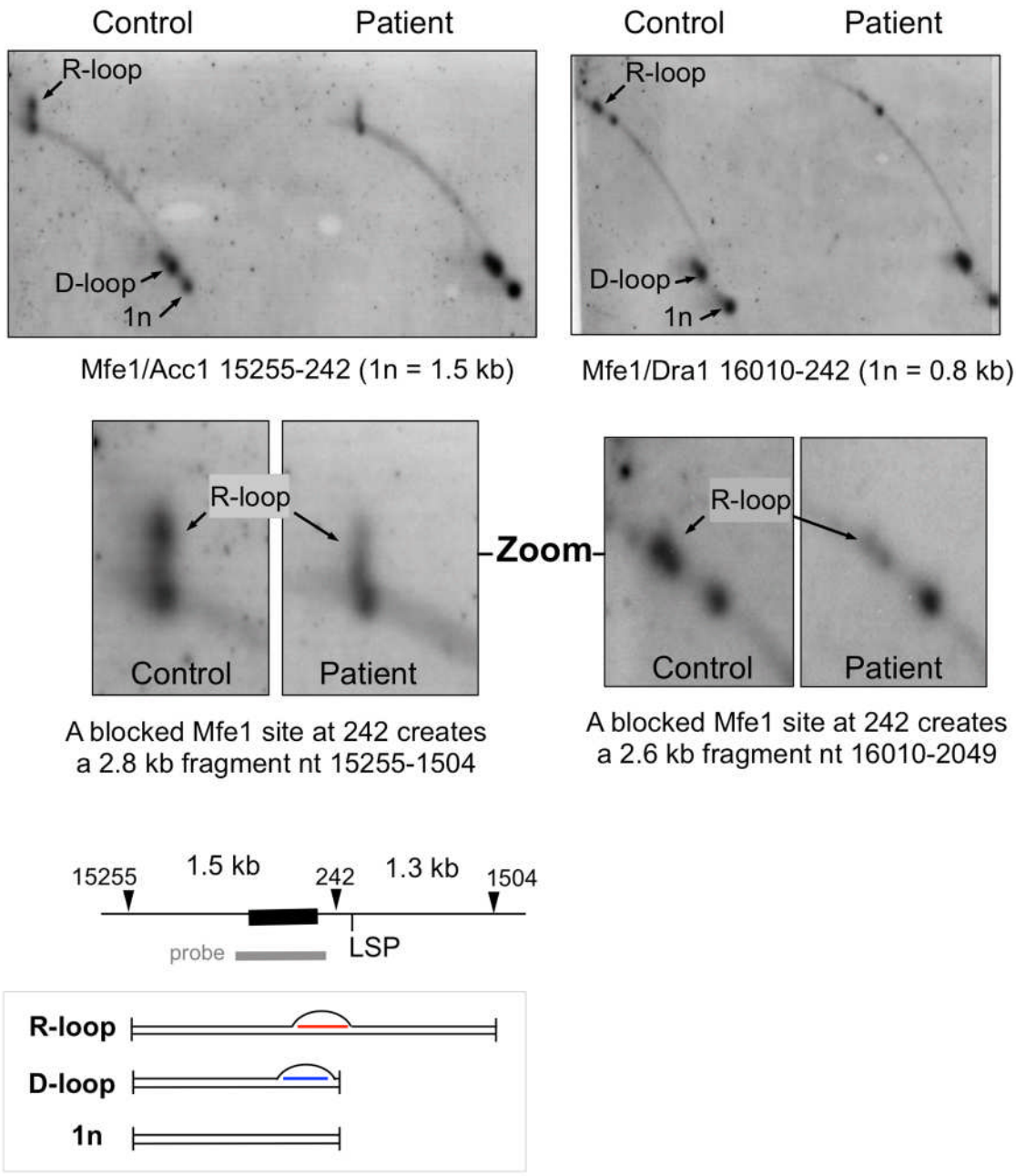

Figure S7. 2D-AGE analysis indicates R-loops are less abundant in fibroblasts with mutant RNase H1 than controls. DNAs from human fibroblasts with wild-type (control) or mutant (V142I) RNase H1 were digested with the indicated restriction enzymes, fractionated by neutral 2D-AGE and blot hybridized to riboprobe h-H15869-168. Cells were subjected to UV/psoralen cross-linking (10 μM TMP, 10 min UV 365 nm) prior to nucleic acids isolation. The control fibroblasts for these experiments derived from a different individual to those used in the 1D-AGE, R-loop assay (Fig. 6C). On average R-loop abundance was ~6 fold lower in V142I fibroblasts than the two control cell lines tested (n = 3 independent experiments).

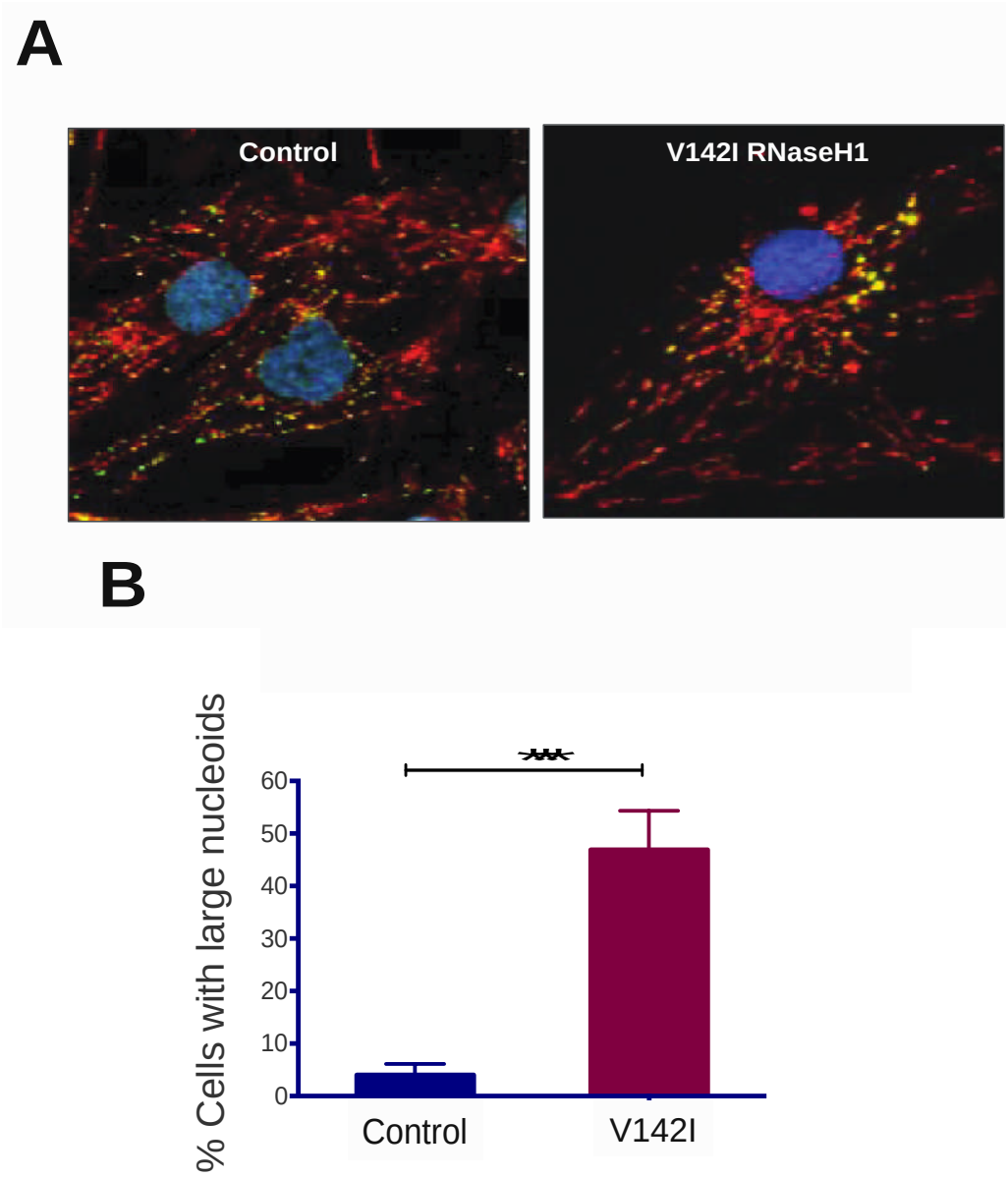

Figure S8. V142I RNase H1 is associated with enlarged mtDNA foci in human fibroblasts. (**A**) An example of the pronounced mtDNA clustering in V142I RNase H1 cells compared with control fibroblasts (7301) imaged by confocal microscopy after incubation with antibodies to the mitochondrial outer membrane protein TOM20 (red) and to DNA (green), merged images are shown. The control fibroblasts for these experiments derived from a different individual to those shown in Fig. 7. The number of cells displaying clustering of mtDNA and its extent were much higher in V142I cells compared to six other fibroblast lines (three of which have a potential or confirmed mitochondrial disorder - thereby excluding generalized mitochondrial dysfunction as a cause of mtDNA aggregation). (**B**) The proportion of cells with mtDNA foci larger than the modal 0.3 µm in a representative control cell line compared with fibroblasts with V142I RNase H1 (n = 4 independent experiments, error bars are standard deviation from the mean). Unpaired two-tailed t test with Welch's correction, p = 0.0008.

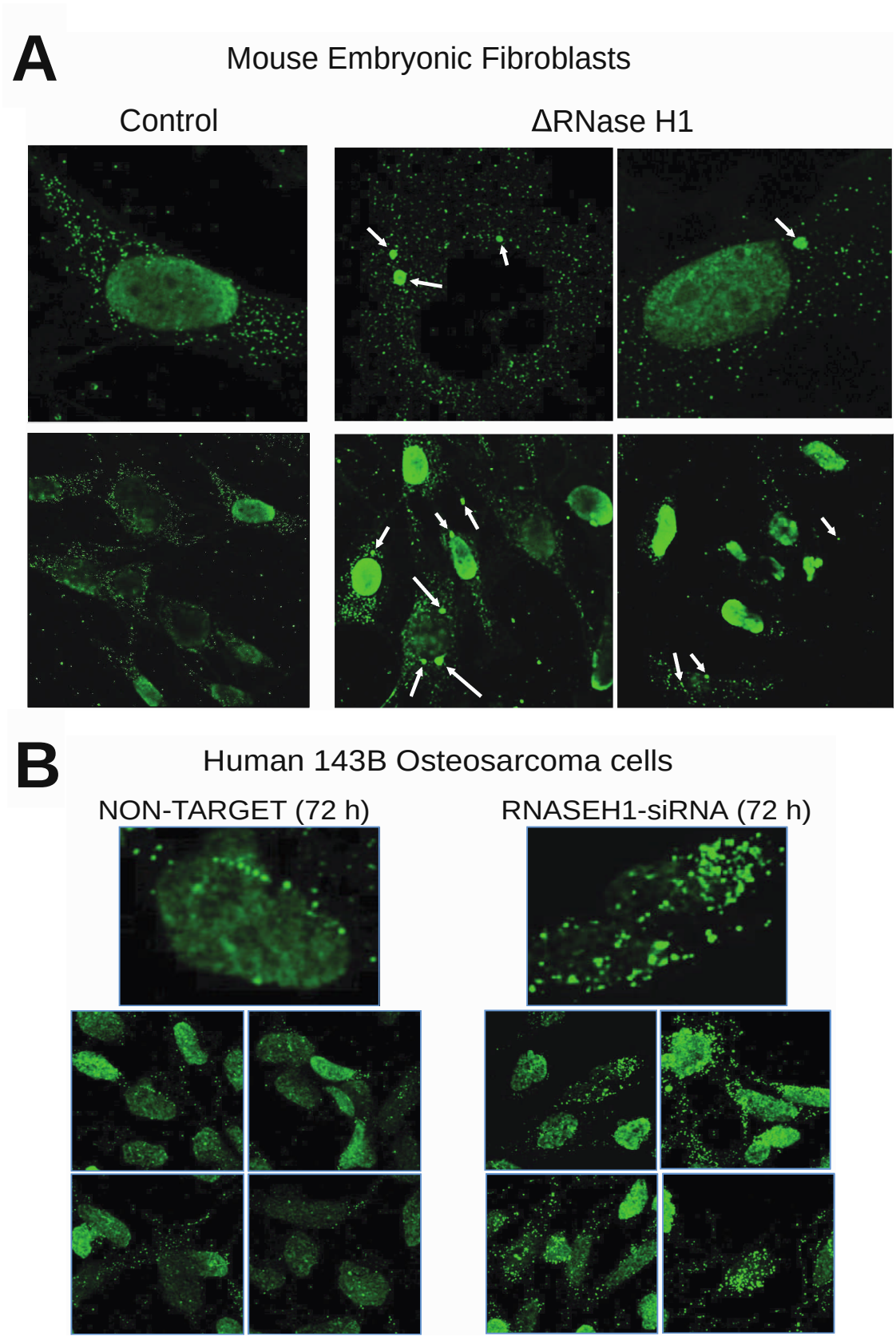

Figure S9. RNase H1 ablation in murine fibroblasts or knockdown in human osteosarcoma cells results in the formation of enlarged mitochondrial DNA foci. MEFs were cultured without (Control) or for 5 or 7 days with 4-hydroxy-tamoxifen (ΔRNase H1) (as previously (10)). Human 143B cells were transfected with a non-target siRNA or siRNA to RNASEH1, and imaged 72 hours later.

Immunocyto-chemistry was performed with anti-DNA antibodies (green). White arrows indicate examples of enlarged mtDNA foci.

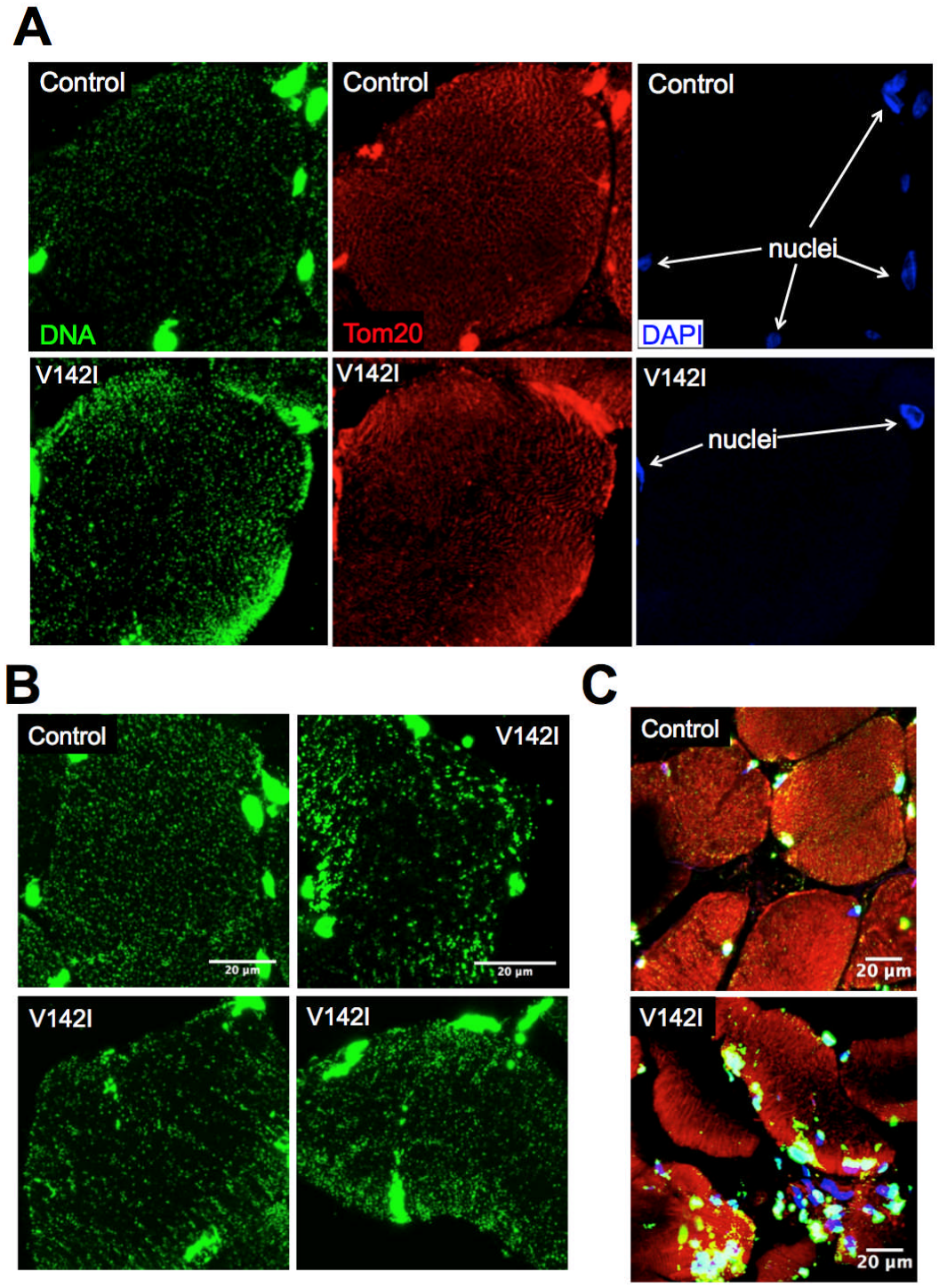

Figure S10. V142I RNase H1 quiescent cells and muscle display mtDNA disorganization and aggregation. (**A**) Individual components of the merged images of Fig. 8B and DAPI-labeled nuclei. (**B**) additional images of individual muscle fibers labeled with anti-DNA antibodies (green); and (**C**) muscle sections of a control and the index case with V142I RNase H1. Anti-DNA - green, Anti-TOM20 (mitochondria) - red. The sizes of the mtDNA foci in muscle sections of the control were 0.25-0.38 μm, similar to those of control fibroblasts (Fig. 7). The nuclei in muscle are denser than in fibroblasts and other cultured cells, which we infer accounts for the non-specific labeling of some nuclei with anti-TOM20. Purple signal in (**C**) is autofluorescence.

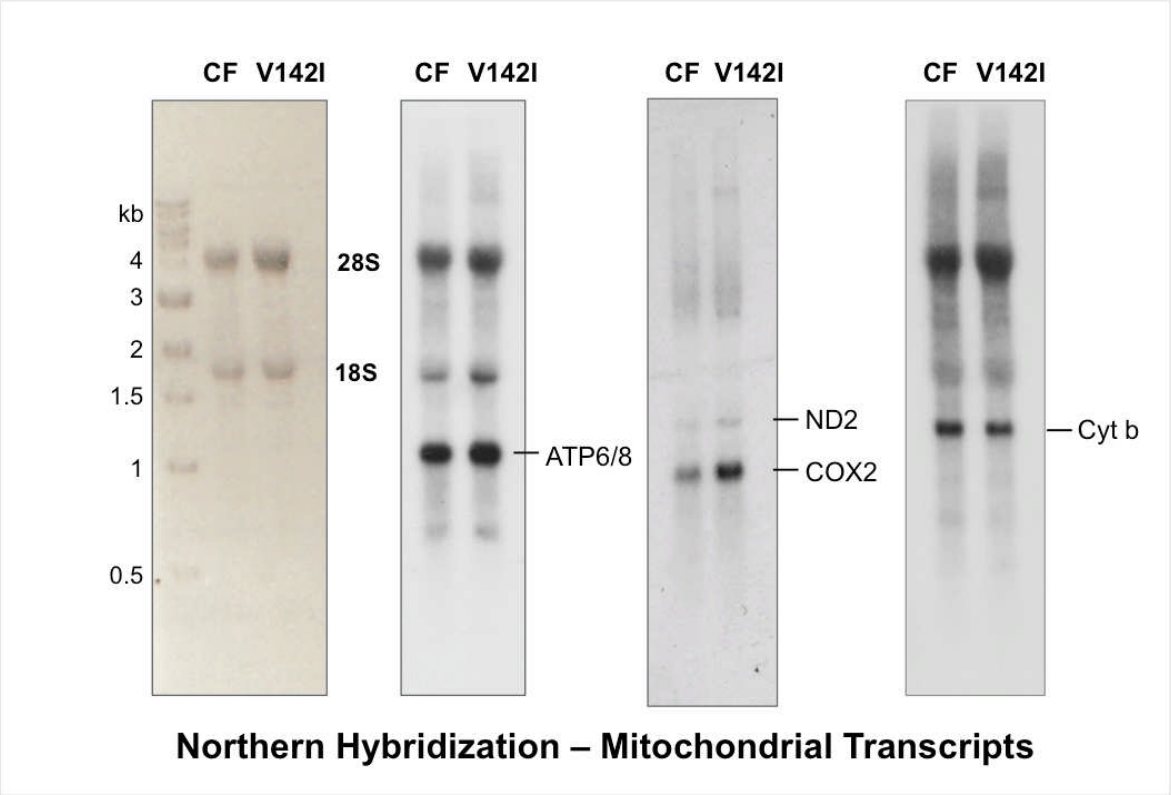

Figure S11. V142I RNase H1 does not decrease the levels of four mature mitochondrial mRNAs or their precursors. RNA was isolated from patient-derived (V142I) and control (CF – L1068) fibroblasts. Five microgram lots were fractionated by 1D-AGE in MOPS buffer (see Materials and Methods) and blot hybridized to ribobprobes complementary to mitochondrial mRNAs encoding ATP synthase subunits 6 and 8 (ATP6/8), NADH dehydrogenase 2 (ND2), cytochrome oxidase subunit 2 (COX2) and cytochrome b (cyt b). The ATP6/8 and cyt b probes also bound non-specifically to the abundant 28S and 18S rRNAs of cytosolic ribosomes.

References

1. Reyes A, *et al.* (2011) Actin and myosin contribute to mammalian mitochondrial DNA maintenance. *Nucleic Acids Res* 39(12):5098-5108.
2. Yang MY, *et al.* (2002) Biased incorporation of ribonucleotides on the mitochondrial L-strand accounts for apparent strand-asymmetric DNA replication. *Cell* 111(4):495-505.
3. Yasukawa T, *et al.* (2006) Replication of vertebrate mitochondrial DNA entails transient ribonucleotide incorporation throughout the lagging strand. *EMBO J* 25(22):5358-5371.
4. Dalla Rosa I, *et al.* (2016) MPV17 Loss Causes Deoxynucleotide Insufficiency and Slow DNA Replication in Mitochondria. *PLoS genetics* 12(1):e1005779.
5. Dalla Rosa I, *et al.* (2014) MPV17L2 is required for ribosome assembly in mitochondria. *Nucleic Acids Res* 42(13):8500-8515.
6. Ruhanen H, Ushakov K, & Yasukawa T (2011) Involvement of DNA ligase III and ribonuclease H1 in mitochondrial DNA replication in cultured human cells. *Biochim Biophys Acta* 1813(12):2000-2007.
7. Bayona-Bafaluy MP, *et al.* (2003) Revisiting the mouse mitochondrial DNA sequence. *Nucleic Acids Res* 31(18):5349-5355.
8. Di Re M, *et al.* (2009) The accessory subunit of mitochondrial DNA polymerase gamma determines the DNA content of mitochondrial nucleoids in human cultured cells. *Nucleic Acids Res* 37(17):5701-5713.
9. Reyes A, *et al.* (2013) Mitochondrial DNA replication proceeds via a 'bootlace' mechanism involving the incorporation of processed transcripts. *Nucleic Acids Res* 41(11):5837-5850.
10. Holmes JB, *et al.* (2015) Primer retention owing to the absence of RNase H1 is catastrophic for mitochondrial DNA replication. *Proc Natl Acad Sci U S A* 112(30):9334-9339.